Journal of FISH BIOLOGY
Published for the Fisheries Society of the British Isles

Journal of Fish Biology (2012) **80**, 1904–1939
doi:10.1111/j.1095-8649.2012.03266.x, available online at wileyonlinelibrary.com

Muscle function and swimming in sharks

R. E. Shadwick* and J. A. Goldbogen

Department of Zoology, University of British Columbia, 6270 University Boulevard, Vancouver, British Columbia, V6T 1Z4 Canada

The locomotor system in sharks has been investigated for many decades, starting with the earliest kinematic studies by Sir James Gray in the 1930s. Early work on axial muscle anatomy also included sharks, and the first demonstration of the functional significance of red and white muscle fibre types was made on spinal preparations in sharks. Nevertheless, studies on teleosts dominate the literature on fish swimming. The purpose of this article is to review the current knowledge of muscle function and swimming in sharks, by considering their morphological features related to swimming, the anatomy and physiology of the axial musculature, kinematics and muscle dynamics, and special features of warm-bodied lamnids. In addition, new data are presented on muscle activation in fast-starts. Finally, recent developments in tracking technology that provide insights into shark swimming performance in their natural environment are highlighted.

Key words: fast-starts; lamnid kinematics; migration; muscle activation; myomeres; tagging.

INTRODUCTION

Sharks are a fascinating and ancient group of fishes. Their locomotor systems have many similarities to those of teleosts, but clearly represent a more primitive or less-derived mechanical design in many ways. Most of the studies of fish muscle and locomotion have been carried out on teleosts, probably due to the ease of obtaining experimental specimens, as sharks are not readily available from aquaculture sources. Thus, all studies of shark muscle and swimming mechanics are on wild-caught specimens, and this seems unlikely to change. Advances in capture, holding and experimental techniques, however, have provided much new information and helped clarify the similarities and differences in organization of the axial musculature, the mechanical properties of the fast and slow fibre types, the swimming kinematics and the muscle activation patterns in sharks, as compared to teleosts. Most new experimental data relate to muscle function in steady swimming, with details on unsteady swimming lagging. Studies of sharks at sea based on digital recording devices are now providing extensive information on locomotor performance on daily or longer timescales. Recent investigations of the anatomical and physiological specializations for high-performance locomotion in lamnids have revealed a remarkable convergence with tunas, their teleost counterparts with respect to form, function, evolution and

*Author to whom correspondence should be addressed. Tel.: +1 604 827 3149; email: shadwick@zoology.ubc.ca

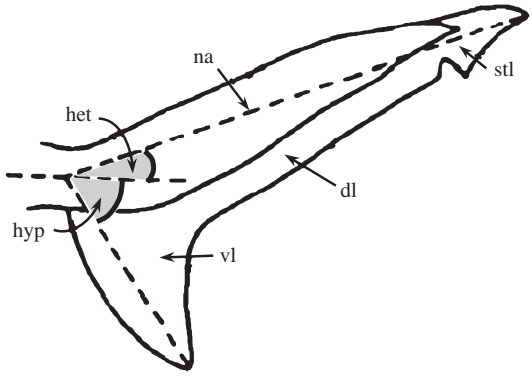

FIG. 1. Diagram of a generalized heterocercal shark tail to illustrate morphological features: the upturned notochord axis (na), the dorsal (dl) and ventral (vl) fin lobes, the small subterminal lobe (stl) and the heterocercal (het) and hypochordal (hyp) angles (modified from Thomson & Simanek, 1977, with permission from Oxford University Press).

ecological niche. Here, current understanding of how shark muscle works and how it is used to power swimming in this diverse group of fishes is reviewed.

BODY MORPHOLOGY RELATED TO SWIMMING

Sharks are morphologically and biomechanically diverse, with body forms ranging from slender and flexible benthic shapes to much more stiff-bodied pelagic types. Thomson & Simanek (1977) compared the morphology of a large number of shark species, particularly in the context of the caudal fin (Fig. 1). They described a range of tail shapes that, although based on a common plan, display extremes represented by the crescent-shaped or lunate tails of Lamnidae to the nearly straight tail of benthic sharks such as Scyliorhinidae. From their analysis, they recognized four patterns of morphology that can also be related to swimming styles in most cases: (1) large, fast-swimming pelagic sharks (Lamnidae) [Fig. 2(a)] and the whale sharks *Rhincodon typus* Smith 1828 with a high aspect ratio (*i.e.* span ÷ chord width) tail, a conical head, a lateral keel on the caudal peduncle; (2) generalized swimmers such as the Carcharhinidae [Fig. 2(b)], with lower heterocercal angles, a flattened ventral surface on the head and no caudal fluke; (3) slow-swimming demersal and benthic species such as Scyliorhinidae [Fig. 2(c)] with very low, almost straight tail, and absent ventral hypochordal lobe and (4) squalomorphs [Fig. 2(d)] which are distinct in their absence of the anal fin, the presence of a well-developed epicaudal lobe and often an elevated insertion of the pectorals.

The marked heterocercal caudal fin of many shark species has long been thought to produce asymmetrical hydrodynamic forces that result in an upward-directed lift force on the tail during forward swimming (Breder, 1926; Grove & Newell, 1936; Alexander, 1965), and a torque about the centre of mass tending to tilt the head downward (classical model). This was hypothesized to be countered by an equal and opposite torque generated by upward lift from the pectoral fins (Harris, 1936; Alexander, 1965; Fish & Shannahan, 2000). Both torques are predicted to increase

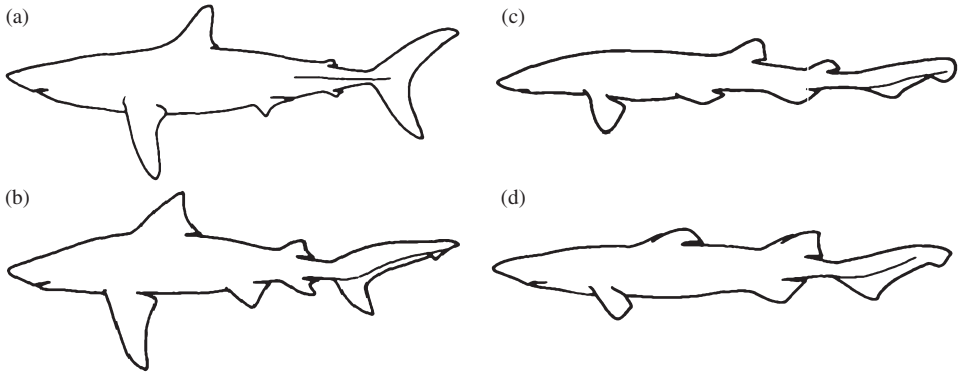

FIG. 2. Representative sharks of the four groups identified by Thomson & Simanek (1977): (a) *Isurus oxyrinchus,* (b) *Carcharhinus leucas,* (c) *Scyliorhinus torrei* and (d) *Centroscyllium fabricii* (modified from Thomson & Simanek, 1977, with permission from Oxford University Press).

in tandem with swim speed so that the net lift force on the body is just equal to the weight of the shark in water. This model is based on the expectation that the larger and stiffer dorsal lobe should lead the ventral lobe in its lateral motions, adopting an angle of attack that results in upward directed lift. Furthermore, the larger dorsal lobe area should result in net forward thrust force acting in a line that is dorsal to the centre of mass, lifting the tail and driving the head down. Although an alternative model in which the lateral motions of the shark tail produce downward lift force causing the head to turn up has been presented (Thomson, 1976), recent evidence from 3-D kinematic analysis of swimming in the leopard shark *Triakis semifasciata* Girard 1855 (Ferry & Lauder, 1996) and flow visualization of *T. semifasciata* and the bamboo shark *Chiloscyllium punctatum* (Müller & Henle 1838) (Wilga & Lauder, 2000, 2002, 2004) do not support this. These studies show convincingly that in small sharks (17–38 cm total length, L_T) swimming slowly (1–1·2 L_T s^{-1}) the tail produces downward and posterior vortex jets, tending to rotate the head downward. Interestingly, they also show that this torque is balanced, not by lift from the pectoral fins, but by lift generated by the body which is held at a positive angle of attack to the flow, while the fins adopt a slight negative angle of attack during steady swimming (Wilga & Lauder, 2000, 2002, 2004; Fig. 3). More recently, Flammang (2010) has shown the importance of the radialis muscle in the caudal fin in altering its shape during locomotion. Whether this kinematic pattern persists in larger individuals swimming at faster speeds remains to be seen.

The situation is probably quite different in lamnids where the lunate caudal fin is much less asymmetrical and more rigid [Reif & Weishampel, 1986; Fig. 2(a)]. The plan area of the caudal fin was measured in four species of Lamnidae and the ratio of dorsal to ventral lobes was found to be *c*. 1·4–1·5 in the shortfin mako *Isurus oxyrinchus* Rafinesque 1810 and the porbeagle *Lamna nasus* (Bonnaterre 1788), and only 1·1–1·2 in the salmon shark *Lamna ditropis* Hubbs & Follett 1947 and the white shark *Carcharodon carcharias* (L. 1758) (R. E. Shadwick, pers. obs.). Furthermore, experiments on excised tails from three specimens of *C. carcharias* (Lingham-Soliar, 2005) indicated that the ventral lobe had up to two-fold greater flexural stiffness. These experiments were, however, conducted on previously frozen tails and freezing

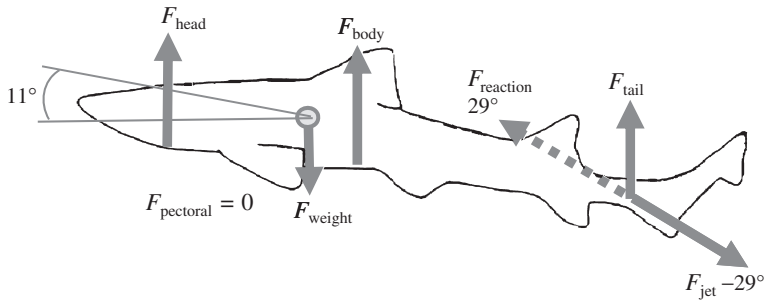

FIG. 3. Proposed model of forces acting on a *Triakis semifasciata* swimming at 1·0 total length s^{-1}, while maintaining horizontal position. ○, the centre of mass; ⟶, force vectors. Lift is generated by the anterior body (F_{head}) and at tail (F_{tail}). The jet generated by the tail motion (F_{jet}) is directed posteriorly and downward at −29°, resulting in a reaction force ($F_{reaction}$) directed anteriorly and upward. In level swimming, the body is held at *c*. 11° to the path of flow, and the pectoral fin force ($F_{pectoral}$) is negligible (modified from Wilga & Lauder, 2002 with permission from the Company of Biologists).

may have a significant effect on passive stiffness, as was shown in the case of the tail of a tope shark *Galeorhinus galeus* (L. 1758) (Alexander, 1965). Given a lack of experimental data on the forces produced by this tail during swimming, it is possible that the net vertical lift forces are generated from the lateral motion of the dorso-ventrally flattened caudal peduncle rather than the caudal fin *per se* as observed in non-lamnid sharks.

THE LOCOMOTOR MACHINERY

MYOMERES AND MYOSEPTA

The segmented axial muscle used in undulatory locomotion in sharks is morphologically similar to muscle in teleosts. A series of myomeres along each side of the body, one per vertebra, form complex, three-dimensionally folded structures with one main anterior-projecting cone and two posterior-projecting cones (Greene, 1913; Nursall, 1956; Alexander, 1969; Gemballa *et al*., 2003; Fig. 4). In this arrangement, each myomere spans several vertebral segments by nesting of the cones, which appear as concentric rings in a body cross-section (Fig. 4). The shapes of myomeres vary not only among different groups of fishes but also at different axial positions along the body, primarily due to accommodation of the body cavity in the pre-anal region and variation in body cross-sectional shape (Nursall, 1956; Gemballa *et al*., 2003). The connective tissue sheets that separate myomeres are the myosepta. It has long been recognized that the myosepta must function as tendons to direct muscle forces to the skeleton (Wainwright, 1983; Reif & Weishampel, 1986; Videler, 1993; Westneat *et al*., 1993; Westneat & Wainwright, 2001). More recently, Gemballa *et al*. (2003, 2006), using micro-dissection, histology, polarized light microscopy and three-dimensional reconstructions, elegantly demonstrated that the myoseptal sheets contain tracts of robust collagen fibres that function as tendons to transfer muscle forces to the axial skeleton. The myoseptal cones are connected by longitudinally oriented epaxial and hypaxial lateral tendons that lie along the surface

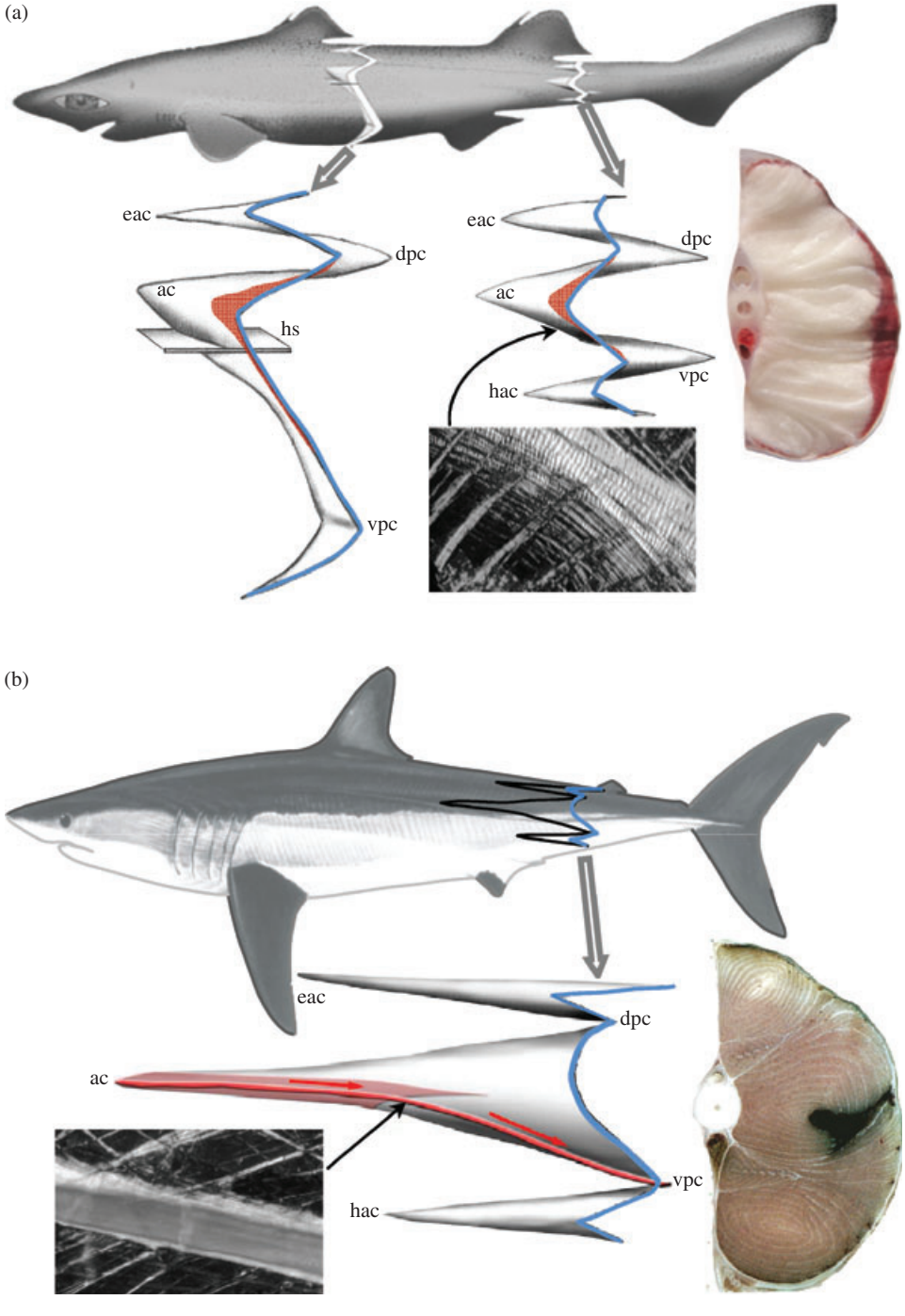

FIG. 4. Legend on next page.

of the anterior cones, and myorhabdoid tendons that lie on the posterior cones. Mediolaterally oriented tendons connect to the vertebral column and the skin (Gemballa *et al*., 2006). Each lateral tendon spans only 5–7·5% of L_T or five to six vertebral segments. Superficial red muscle fibres insert into the mid-region of the lateral tendons on each myoseptum (Gemballa *et al*., 2006); thus, their contractions cause local bending of the body. These anatomical features are similar to those in teleosts, suggesting that the basic myoseptal anatomy evolved early in gnathostome history (Gemballa *et al*., 2003, 2006).

Elongation of myomeres and their associated myosepta in more derived fishes (*e.g.* lamnids and tunas) results in a greater number of vertebrae spanned and more numerous concentric rings seen in cross-section [Fig. 4(b)]. For example, in *I. oxyrinchus* the posterior myomeres are highly elongated, with the most prominent tendon being the thick lateral tendon on the hypaxial surface of the anterior-pointing cone [Fig. 4(b)]. These cones are so elongated that their lateral tendons span up to 24 vertebral segments, or 19% of L_T, from the tips of the anterior cones through the posterior cones and into the skin in the region of the caudal peduncle (Gemballa *et al*., 2006) [Fig. 4(b)]. This unique anatomy is the basis of the special swimming mode in lamnids.

MUSCLE FIBRE TYPES

A casual glance at the lateral muscle of a transversely sectioned shark or teleost reveals two differently coloured muscle groups [Fig. 4(a)], a narrow band of dark or red fibres lies just under the skin [except for lamnids; Fig. 4(b)], while the remainder is much lighter or white. This colour distinction arises from differences in vascularization and myoglobin content (Kryvi *et al*., 1981; Totland *et al*., 1981) that reflect functionally different contractile properties, first described in studies on sharks (Bone, 1966, 1978). The red muscle is aerobic and designed for slow, continuous swimming, whereas the white muscle is generally anaerobic and suited for brief bursts of speed or fast-starts. This functional distinction is also evident from differences in mitochondrial content (Kryvi & Eide, 1977; Bone *et al*., 1986), mitochondrial oxidative enzymes and Ca^{2+}-activated myosin ATPase activities (Kryvi & Totland, 1977; Bone, 1989) (Table I). Although additional minor fibre types have been identified in

FIG. 4. The organization of the lateral muscle in sharks. (a) *Etmopterus spinax*, a typical ectothermic subcarangiform species. The body is long and slender and has a long heterocercal tail. A post-anal cross-section shows that the bulk of muscle is fast, pale fibres, while the aerobic red fibres occupy a thin band just under the skin. Anterior and posterior myosepta are shown, in their original positions in the body and enlarged for detail. The lateral edge of each myoseptum that links to the skin is delineated in blue. Lower inset is a polarized light micrograph showing a portion of the lateral tendon on the hypaxial surface of the posterior myoseptum. (b) *Isurus oxyrinchus* has a thick streamlined body with a tapered caudal region and a large lunate tail fin. A post-anal cross-section shows that the aerobic red fibres (dark area) are internalized and lie on the anterior-pointing cones. One posterior myoseptum is shown to emphasize the difference from the non-lamnid example, in particular the very elongated anterior cones. Here, the red fibres (in pink) are seen inserting into a major lateral tendon (red, ⟶) on the hypaxial surface of the anterior cone. The inset polarized light micrograph shows the thick lateral tendon. ac, anterior-pointing cone; eac, epaxial anterior cones; hac, hypaxial anterior cones; dpc, dorsal posterior cones; vpc, ventral posterior cones; hs, horizontal septum. Redrawn from Gemballa *et al*. (2006) with permission from John Wiley and Sons.

TABLE I. Comparison of slow and fast muscles in sharks (Bone, 1978, 1989; Bone *et al*., 1986)

Slow (red) fibres	Fast (white) fibres
Smaller diameter (20–50% of fast)	Large diameter (100–150 μm)
Well vascularized, abundant myoglobin, abundant large mitochondria, red colour	Poorly vascularized, little or no myoglobin, low mitochondrial volume density, usually white
Oxidative enzyme systems	Enzymes of anaerobic glycolysis
Low activity of Ca^{2+}-activated myosin ATPase	High activity of myosin ATPase
Stored lipid and glycogen, sarcotubular system less in volume than in fast fibres	Glycogen stored, usually little lipid, relatively larger sarcotubular system
Multiple (distributive) innervation	Focal, dual innervation
Lower resting potentials *v*. fast fibres	Higher resting potentials
No propagated action potentials, except under experimental conditions	Propagated action potentials
Long-lasting contractions evoked by depolarizing agents	Brief contractions evoked by depolarizing agents
Maximum isometric stress 70–142 kPa[a]	Maximum isometric stress 180–289 kPa[a]
Maximum unloaded shortening rate 1·5–1·8 L_{musc} s^{-1}[a]	Maximum unloaded shortening rate 3·8–4·5 L_{musc} s^{-1}[a]
Power output 8·5–29 Wkg^{-1}[a]	Power output 55–129 Wkg^{-1}[a]
Efficiency in cyclic contractions 51% at 0·74 Hz[b]	Efficiency in cyclic contractions 41% at 2·5 Hz[c]
Cycle frequency for maximum power 1·02 Hz[b]	Cycle frequency for maximum power 3·5 Hz[c]

[a]Data for *Scyliorhinus canicula* (Bone *et al*., 1986; Lou *et al*., 2002).
[b]Curtin & Woledge (1993*b*).
[c]Curtin & Woledge (1993*a*).
L_{musc}, muscle length.

some shark species, the majority of slow swimming is powered by the red fibres, while fast or burst swimming relies on the white fibres (Bone & Chubb, 1978; Totland *et al*., 1981).

Considering Fig. 1 again, it might seem surprising that the quantity of muscle used to power continuous swimming is only a small fraction of the quantity that is required for bursts. Two important factors explain this. First, sharks are only slightly negatively buoyant (body mass in water being only 5% or less than the mass in air; Bone & Chubb, 1978); thus, the effects of gravity are nearly negligible; the body is well streamlined, so drag and the power needed to swim at slow cruising speeds (*c*. 0·3–1 L_T s^{-1}) are relatively low. The minimum speed required to maintain hydrodynamic equilibrium to match body mass is also low (Bone, 1989). Consequently, red fibres typically comprise <10% of the total muscle mass or <5% of the total body mass; Bone (1978) gives average red muscle masses of 8–11% of total muscle mass for the spotted catshark *Scyliorhinus canicula* (L. 1758) and the blue shark *Prionace glauca* (L. 1758). Bernal *et al*. (2003*a*) reported red muscle mass was 2–3% of total body mass in eight species of pelagic sharks, but there is evidence that this ratio may be increased at very large body size (Carey *et al.,* 1985). Most important is the fact that

the thrust power required to swim increases non-linearly with velocity (V). Thrust force must match drag, which increases in proportion to V^2, power (= drag $\times V$) will increase as V^3 (Webb, 1975). For example, a burst speed of four times cruising speed would require *c*. 64 times more muscle power output. White muscle typically has larger cells with greater myofibrillar content, larger force and faster contraction velocities, so muscle power output, the product of force and shortening velocity, is considerably higher (Bone 1978; Table I). In *S. canicula,* mass-specific power output in white muscle is five to six times higher than in red muscle, and white muscle mass is *c*. 10 times greater, so the power available seems to match that needed for burst speeds (Table I).

MECHANICAL PROPERTIES

Mechanical properties of myotomal muscle of sharks were first measured in isolated, chemically skinned fibres from *S. canicula* (Altringham & Johnston, 1982*a*, *b*; Bone *et al*., 1986). These studies yielded data on the force–velocity relation for red and white fibres, which confirmed the roles these two fibre types have in locomotion, as previously inferred by electromyography (EMG) (Bone, 1966). Curtin & Woledge (1988) used intact myotomal muscle preparations from *S. canicula* to investigate basic contractile properties of shark red and white muscle. Maximal instantaneous power can be calculated from experimental force and velocity curves; for *S. canicula,* Curtin & Woledge (1988) calculated that peak power output for white muscle was 91 $\mathrm{Wkg^{-1}}$ at a shortening velocity of *c*. 1 muscle length (L_{musc}) $\mathrm{s^{-1}}$ or about one third of the maximum unloaded shortening velocity. From this power they also predicted that the maximum burst speeds could range up to 12·9 L_{T} $\mathrm{s^{-1}}$ (Curtin & Woledge, 1988), probably much higher than these sharks are capable of attaining. In a more recent study, Lou *et al*. (2002) used vital staining to account for only live fibres in the test bundles, and reported maximum isometric tetanic stress, maximum shortening velocity and maximum instantaneous power for red and white fibres, respectively, as 142 and 289 kPa, 1·8 and 3·8 L_{musc} $\mathrm{s^{-1}}$ and 29 and 120 $\mathrm{Wkg^{-1}}$, both at shortening velocities of 0·3 of the maximum (Table I).

While force–velocity experiments characterize a muscle's intrinsic capacity to develop instantaneous power, they do not shed light on the performance of a muscle in cyclic contractions at different frequencies, such as in swimming, where deactivation is enhanced by shortening, but usually sets an upper limit on the rate at which a muscle can cycle. To more effectively measure muscle properties *in vitro* under conditions that closely mimic function *in vivo*, the work-loop technique is commonly used (Syme, 2006). This was first applied to the study of shark muscle by Curtin & Woledge (1993*a*, *b*), again on white and red fibres from *S. canicula.* By measuring net work and heat produced, they sought to determine the optimal frequency and stimulus timing conditions that produced maximum power and efficiency. They found that for maximum power and maximum efficiency the stimulus must begin while the muscle fibres are being stretched and end before shortening has ended. Interestingly, this is similar to *in vivo* stimulus conditions determined in later experiments on slow-swimming sharks (Donley & Shadwick, 2003; Donley *et al*., 2005). In both red and white fibres, maximum efficiency occurred at a lower frequency than maximum power (Curtin & Woledge, 1993*a*, *b*; Table I), leading to the possibility that power may be maximized *in vivo* at the expense of efficiency

or *vice versa*. This may be an important property that fish take advantage of under differing locomotor demands, and warrants further investigation.

STEADY SWIMMING

KINEMATICS OF UNDULATION

Steady swimming in sharks is powered by a sequential contraction of myomeres alternately along both sides of the body. This generates a propulsive undulatory wave that propagates along the body with increasing amplitude from head to tail (Fig. 5). Each portion of the body involved in the wave imparts momentum to the water in a backward and lateral direction, producing a reaction force that has a forward component contributing to the thrust. But there is also a lateral component that wastes kinetic energy and tends to make the head recoil sideways (Webb, 1975). Although most fishes are well streamlined, the undulation increases drag several-fold compared to the same body moving in a rigid posture, making this form of thrust production relatively inefficient (Webb, 1975).

The first quantitative description of fish swimming kinematics was made in a now-classic study by Gray (1933), which included high-speed ciné movies of a swimming spiny dogfish *Squalus acanthias* L. 1758. Gray (1933) described the

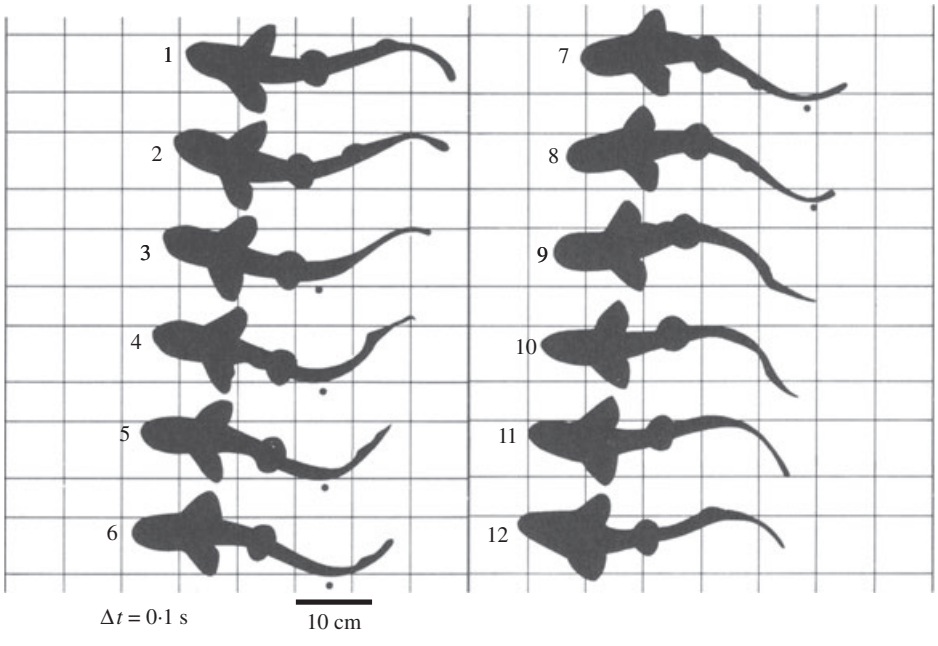

FIG. 5. Images from frames of a high-speed ciné film of a swimming *Squalus acanthias*, showing the propulsive wave on the body. Tracking a lateral wave peak, as indicated by ●, shows that the wave travels backward on the body, but also back relative to the water as the fish moves forward. This demonstrates that the propulsive wave speed is greater than the fish's swimming speed. Time interval between frames is 0·1 s. Redrawn from Gray (1933), with permission from the Company of Biologists

undulatory motion of *S. acanthias* as being similar to that in teleosts such as whiting *Merlangius merlangus* (L. 1758) and eel *Anguilla anguilla* (L. 1758). He showed that in steady forward swimming the undulatory wave travels backward at a velocity (V) that is always greater than the forward velocity of the fish (U). The distance travelled forward in one tail-beat cycle is the stride length, λ_s. If the path traced through the water by the tail tip (or any other segment of the body) is considered as representing a wave of forward movement (Fig. 6), then λ_s is the wavelength of progression and is equal to the velocity U times the cycle period T or, Uf^{-1} where f is tail-beat frequency. For most fishes, including sharks, measured values of λ_s fall in the range of 0·6–0·7 of L_T for steady swimming (Wardle *et al*., 1995; Shadwick & Gemballa, 2006). To generate forward thrust, the propulsive wave must push on the water, but because the water gives way the wave must travel backwards along the body relative to the water to generate thrust, *i.e*. V is always $>U$ (Fig. 6). Consequently, the length of the propulsive wave on the body λ_b is greater than λ_s, and the path angle of a body segment is greater than the orientation of the segment relative to the direction of forward travel [Fig. 6(b), (c)]. This ensures that the segment has a lateral component of motion relative to the flow, *i.e.* a positive attack angle α [Fig. 6(c)] (Webb, 1975; Jayne & Lauder, 1995). Experimental measurements of α during swimming are difficult to obtain and limited. Bainbridge (1958) showed that in goldfish *Carassius auratus* (L. 1758) and dace *Leuciscus leuciscus* (L. 1758) α at the tail tip and caudal peduncle ranged up to 30° and was positive for *c*. 75% of the tail-beat cycle. Similarly, a study on largemouth bass *Micropterus salmoides* (Lacépède 1802) found that α ranged up to 20° and was positive for *c*. 68% of a cycle (Jayne & Lauder, 1995). There are no recorded data for α in any swimming shark but, given the shape and high flexibility of their tails, this may not be a useful measurement. The ratio $U{:}V$ $(= \lambda_s{:}\lambda_b)$ defines the slip of the body in the water. In forward swimming, slip values $<1{\cdot}0$, the propulsive wave travels faster than the body and generates forward and lateral thrusts. When U approaches V, α decreases because the path of the segment coincides closer to the shape of the propulsive wave. If $U = V$, the propulsive and progression waves are coincident, $\alpha = 0$, there is no relative motion between the body wave and the water, and no thrust is generated (Webb, 1975). If $U{:}V > 1{\cdot}0$, then the body wave would travel forward relative to the water and the fish would decelerate. The propulsive (*i.e.* Froude) efficiency is the ratio of thrust power:total power output, which can be expressed as $(U + V)\,(2V)^{-1}$ (Webb, 1975; Webb *et al*., 1984). When U is close to V the locomotor efficiency is optimized because the energy lost to lateral motion is minimized. For example, Froude efficiency would be 0·75 when $U{:}V = 0{\cdot}5$, rising to 0·95 for $U{:}V = 0{\cdot}9$. Gray's (1933) data for *S. acanthias* gave an efficiency of 0·53. Generally, λ_b is *c*. 1·0 L_T, so $U{:}V$ is *c*. 0·7, although this often decreases at speeds below 1 $L_T s^{-1}$ (Hunter & Zweifel, 1971; Wardle *et al*., 1995; Lowe, 1996; Shadwick & Gemballa, 2006). Consequently, the Froude efficiency is also decreased at low swim speeds.

Hunter & Zweifel (1971) found that the tail-beat frequency of a smoothhound shark *Mustelus henlei* (Gill 1863) swimming in a flume increased linearly with increases in swim speed, while the amplitude remained at *c*. 0·2 L_T. Webb & Keyes (1982) analysed the propulsive movements of several species of sharks swimming in large tanks at an aquarium. They found that, as in teleosts, the relationship between speed and tail-beat frequency was linear, but they also found evidence that

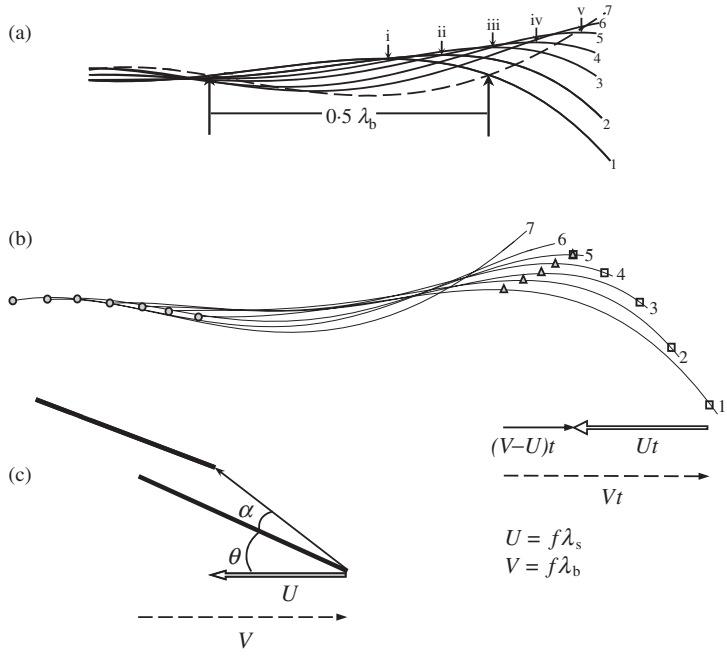

FIG. 6. Curves representing body midlines from successive 60 Hz video images of a swimming fish to show how V (propulsive wave velocity) or λ_b (the propulsive wavelength) can be measured. (a) By aligning the midlines on the horizontal axis, the position of peaks in lateral deflection can be followed in time (⟶, i–v), each separated by a time interval of 16·67 ms. In this example, the deflection peak travels 0·35 lengths (L) in 66·7 ms, yielding $V = 5{\cdot}2\ L\ s^{-1}$; the tail-beat frequency is 4·5 Hz, giving $\lambda_b = 1{\cdot}15\ L$. Alternatively, the distance on the body between nodes of the body wave depicted by the intersection of midlines (⟹) from the start of successive half tail beats yields a measurement of half λ_b; in this example $\lambda_b = 1{\cdot}1\ L$, giving $V = 5{\cdot}0\ L\ s^{-1}$, very similar to the first method. (b) Midlines as in (a), here displaced horizontally to indicate the forward movement of the fish. The distance travelled forward through space by a point on the body (*e.g.* □ at the tail tip or ○ at nose) is represented by Ut, where t is time, the distance travelled backward along the body by the crest of the propulsive wave is Vt, while the difference in these quantities $(V - U)t$ represents the relative progression of the wave crest (△) backward in space. (c) The position of a tail segment at two successive times showing its forward and lateral movements. Its orientation relative to forward progression of the body is the angle θ. The angle of attack of the segment relative to the fluid flow is α. The path angle of the segment is $(\alpha + \theta)$. When U approaches V, α decreases. If $U = V$, $\alpha = 0$ and no thrust is produced. λ_s is the wavelength of the path traced out by the body of the fish (*i.e.* the stride length).

modulation of tail-beat amplitude and the length of the propulsive wave could influence speed. Lowe (1996) found that hammerhead sharks *Sphyrna lewini* (Griffith & Smith 1834) swimming freely in a pond increased their tail-beat frequency linearly with speed, up to U_{crit}, the maximum aerobic speed. A common feature of swim tunnel trials with sharks is that they swim with a narrow range of speeds, generally no higher than 0·5–1 $L_T s^{-1}$ (Hunter & Zweifel, 1971; Graham *et al.*, 1990; Lowe, 1996; Donley & Shadwick, 2003; Donley *et al.*, 2005), relatively slow compared to many teleosts. Records of sharks swimming at sea or in large enclosures also indicate low routine speeds on the order of 0·3–0·4 $L_T\ s^{-1}$ (Weihs *et al.*, 1981; Lowe, 1996; Klimley *et al.*, 2002; Sundström & Gruber, 2002).

MUSCLE FUNCTION IN STEADY SWIMMING

Non-lamnid sharks

Beyond differences in the function of the two major muscle fibre types with respect to swimming speed, recent studies on teleosts have revealed significant variation in how the lateral muscles are activated in relation to their shortening cycle and position along the body. For example, it has commonly been observed that the wave of muscle activation (measured by EMG) propagates along each side of the body faster than the wave of body bending or muscle shortening (*i.e.* strain), leading to perceived differences in the pattern of force development with longitudinal position (Shadwick & Gemballa, 2006). Commonly, muscle fibres are activated before reaching their peak length *in vivo* and deactivated while shortening; this has been shown to optimize work and power output by increasing force and enhancing relaxation between cyclic

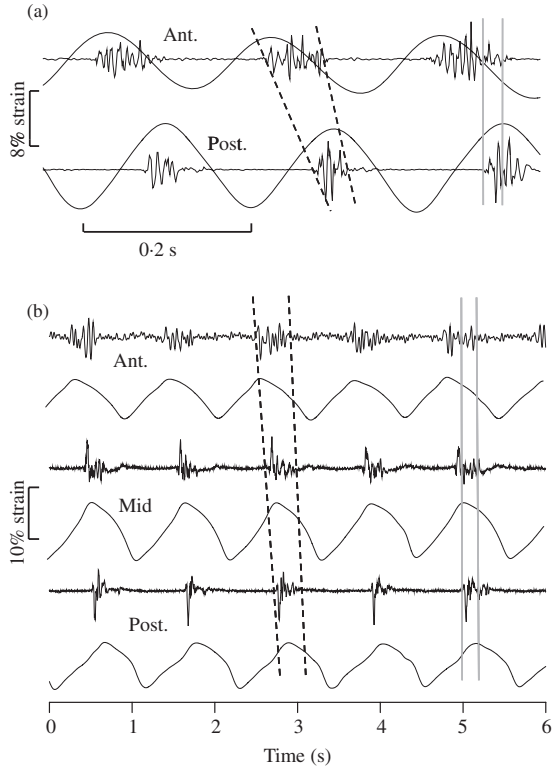

FIG. 7. (a) Red muscle activation strain at anterior (Ant.) (0·43 total lengths, L_T) and posterior (Post.) (0·75 L_T) locations in a *Scomber japonicus* swimming at 3·0 L_T s^{-1}. - - -, the onset and offset of activation which occur later in time posteriorly, but earlier relative to the peaks of strain. ——, a period in one tail-beat cycle when anterior muscle is actively shortening while posterior muscle is stretched as it is activated (R. E. Shadwick, unpubl. data). (b) Red muscle activation and strain, measured by sonomicrometry, at anterior (Ant.) (0·42 L_T), mid (Mid.) (0·61 L_T) and posterior (Post.) (0·72 L_T) locations in *Triakis semifasciata* swimming at *c*. 0·5 $L_T s^{-1}$. Activation occurs later towards the posterior but, on average, the activation duration and phase relative to the strain cycle were not significantly different at the three sites [——, as in (a)]. Redrawn from Donley & Shadwick (2003) with permission from the Company of Biologists.

contractions [Syme, 2006; Fig. 7(a)]. In many fishes, there is also a decrease in the duration of muscle activation in more caudal locations. But the most intriguing feature results from the differences in the propagation of activation and shortening waves, as mentioned above. Specifically, the posterior muscle is activated later in time, but earlier in its shortening phase [Fig. 7(a)], to the extent that posterior muscles are active and being lengthened during a portion of the time in which the anterior muscle is actively shortening. This has led to a number of models of regional variation in muscle function and power production in different species, linked to measured differences in inherent contractile speed related to body position within fibre type, and optimization for different swimming behaviours (Wardle *et al*., 1995; Coughlin, 2002; Shadwick & Gemballa, 2006; Syme, 2006).

Interestingly, only two studies to date have investigated activation timing and strain of red muscle in swimming sharks and neither revealed any axial variation in the duration of muscle activation or its phase with muscle strain (Donley & Shadwick, 2003; Donley *et al*., 2005). In *T. semifasciata*, the EMG duration averaged *c*. 30% of one tail-beat period in locations from 0·42 to 0·72 L_T [Fig. 7(b)] during steady swimming at 0·5–1 L_T s^{-1}. As in many teleosts, activation began during the latter part of muscle lengthening and ended during shortening, but with the same phase (*i.e.* also the same duration) at all locations tested [Fig. 7(b)]. This led to a prediction that, unlike teleosts, there is uniform muscle function along the body in sharks, and regional variation is not necessary for undulatory aquatic locomotion (Gillis, 1998). Myomeres along the body are linked to adjacent vertebrae, so their contractions cause local bending (Donley & Shadwick, 2003; Gemballa *et al*., 2006). The relationship between the amplitude of muscle strain and the amount of bending it causes is dependent on the distance of the muscle fibres from the backbone (*i.e.* the neutral axis of bending), like a simple beam in bending (Katz & Shadwick, 1998; Shadwick *et al*., 1998). In many teleosts, red muscle strains range from *c*. ±3 to ±8% in steady swimming, usually increasing as the propulsive wave amplitude increases caudally (Shadwick & Gemballa, 2006). By comparison, average red muscle strain in *T. semifasciata*, measured by sonomicrometry, increased from ±3·9% at 0·4 L_T to ±6·6% at 0·6 L_T, then decreased to ±4·8% at 0·7 L_T. Although muscle contractions caused a progressive increase in lateral amplitude along the body (Figs 5 and 8), the tapering of the body resulted in a slight decrease in red muscle strain at 0·7 L_T.

Special features of Lamnidae: muscle function in steady swimming

The family Lamnidae consists of five species, *C. carcharias, L. nasus*, *L. ditropis*, *I. oxyrinchus* and the longfin mako *Isurus paucus* Guitart 1966. These species are all highly active pelagic predators that must swim continuously to ventilate and not sink, and that cover large geographical ranges. Lamnids have many anatomical and physiological features that set them apart from other sharks, while at the same time revealing a remarkable similarity to tunas through convergent evolution over the past 50–60 million years (Martin, 1996; Bernal *et al*., 2001*a*, 2003*a*; Donley *et al*., 2004; Shadwick, 2005). Lamnids are distinguished by a thick and streamlined body, highly tapered to a narrow caudal peduncle with a stiff crescent-shaped hydrofoil-like tail fin [Fig. 4(b)]. This is believed to generate thrust by forward-directed hydrodynamic lift (*i.e.* lift-based thrust; Lighthill, 1970; Triantafyllou *et al.,* 1993). This body shape concentrates on the bulk of the locomotor muscle centrally while reducing mass and maximizing lateral motion in the posterior region. The most

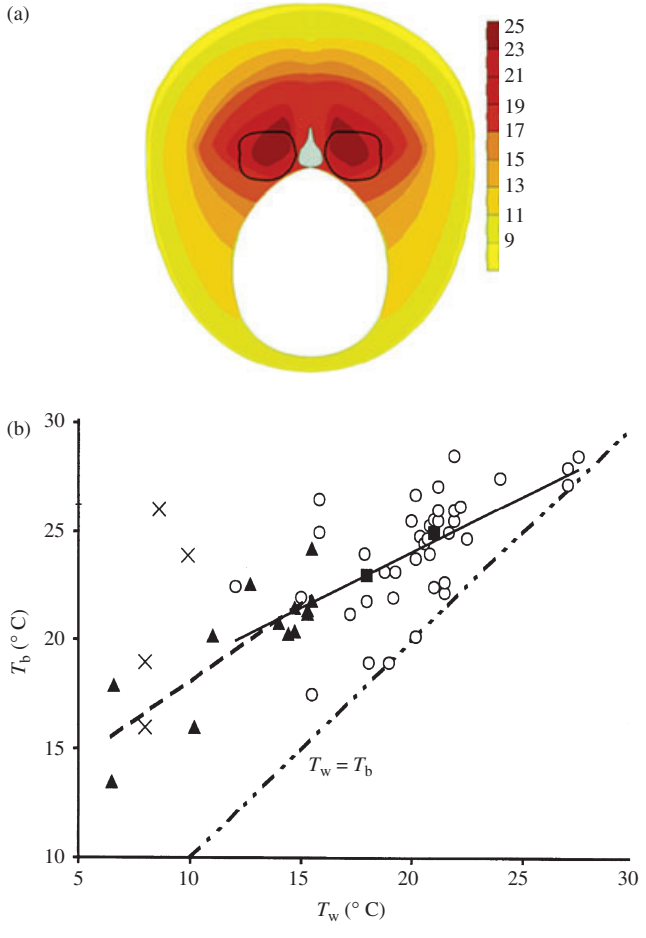

FIG. 8. (a) Temperature profile across the body of the lamnid *Lamna ditropis* at *c*. 0·4 total length, L_T, immediately after capture. Muscle temperature ranges from 25° C in the core red muscle to 9° C just under the skin. Surface water temperature was 8·5°C. Black outlines denote the position of the red muscle (based on data in Bernal *et al.,* 2005). (b) Core body temperatures (T_b) in lamnids are higher than the ambient surface water temperature (T_w) where they were caught. At decreased T_w, the thermal excess is greater, although T_b falls. Regression equation for *Isurus oxyrinchus* [○, ——, $y = 0{\cdot}51x + 13{\cdot}80$ ($r^2 = 0{\cdot}62$, $n = 38$)] and *Lamna nasus* [▲, - - -, $y = 0{\cdot}72x + 10{\cdot}80$ ($r^2 = 0{\cdot}68$, $n = 13$)]. Other species: *L. ditropis* (×), *Carcharodon carcharias* (■). Adapted from Bernal *et al*. (2001*b*) with permission from Elsevier.

well-known specialization found in this group and in tunas is regional endothermy or heterothermy (Carey *et al*., 1985; Block *et al*., 1993; Graham & Dickson, 2000; Katz, 2002). Vascular heat exchangers in the medial red muscle capture heat produced from contractions that power continuous swimming. Muscle heat in outgoing venous blood warms the incoming arterial blood, thereby maintaining the temperature around the red muscle elevated relative to the ambient water [Fig. 8(a)], not to a constant level as in mammals, but to an excess that is diminished with increasing water temperature [Carey *et al*., 1985; Bernal *et al*., 2001*a*; Fig. 8(b)]. These fishes have elevated aerobic metabolism compared to their ectothermic relatives, fuelled by

enhanced capacity to deliver oxygen to muscle and heart tissues, elevated metabolic enzyme activities in muscle and heart, large gill area and large thick-walled hearts (Dickson *et al*., 1993; Bernal *et al*., 2003*b*; Wegner *et al*., 2010).

Another lamnid and tuna innovation is that the loins of aerobic red muscle are situated medially, deep in the body, rather than superficially as in other fishes [Fig. 4(b)]. In addition, the red fibres occupy the tips of the anterior-pointing cones of the highly elongated myomeres [Fig. 4(b)], placing these muscle fibres much more anterior than they would be if they occupied a superficial position in the same myomeres (Gemballa *et al*., 2006; Perry *et al*., 2007; Syme & Shadwick, 2011). Thus, the red muscle is distributed centrally over a relatively narrow longitudinal range, in contrast to the situation of superficial red muscle in ectothermic sharks. For example, in *P. glauca* and *T. semifasciata*, the red muscle is present in appreciable quantity from *c*. 0·25 to 0·85 L_T (Fig. 9), with the maximum cross-section occurring across a broad band from 0·5 to 0·75 L_T; in *L. ditropis*, the red muscle effectively spans from only 0·3 to 0·55 L_T with a sharp peak in cross-section occurring at 0·4 L_T, the thickest part of the body, at the level of the dorsal fin (Bernal *et al*., 2003*a*; Perry *et al*., 2007). This shift in red muscle mass might appear to create a disadvantage for powering continuous swimming because the muscle is far from the tail and close to the bending axis, but instead it turns out to provide substantial benefit. In fact, it is the positioning of red muscle on the anterior myoseptal cones that allows these fibres to link to myoseptal tendons unavailable to superficial fibres [Fig. 4(b)]; ones that can span large numbers of body segments (Donley *et al*., 2004; Gemballa *et al*., 2006), thereby providing the basis for the 'stiff-body' swimming mode that lamnids employ (Bernal *et al*., 2001*b*). That is, the lateral motion of the body is restricted to the caudal region because the centrally located muscles are linked to the caudal region by the long-reaching lateral tendons [Fig. 4(b)], rather than causing local bending as superficial red fibres do in the non-lamnid sharks. For example, Fig. 10 compares relative lateral displacement along the body for swimming *T. semifasciata* and *I. oxyrinchus*. At 0·5

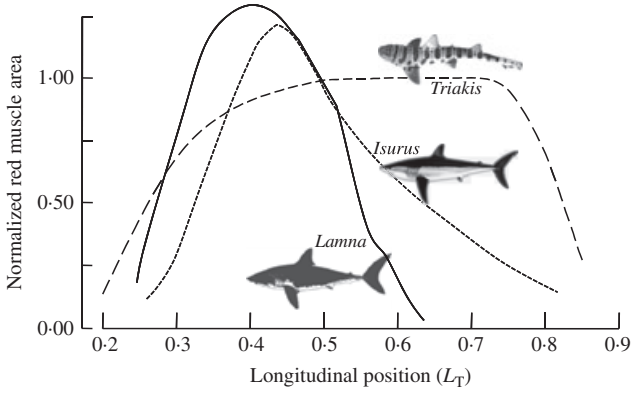

FIG. 9. Red muscle distribution in two lamnids, *Isurus oxyrinchus* (.....) and *Lamna ditropis* (___), and the non-lamnid *Triakis semifasciata* (- - -). Data are based on the area of red muscle measured in cross-sections at different positions along the body, and normalized to the area of red muscle at 0·5 total length, L_T, in each fish to account for differences in body size. In lamnids the red muscle mass is maximal at 0·4–0·5 L_T, while in the non-lamnid the maximum occurs between *c*. 0·5 and 0·75 L_T. The mass of red muscle is *c*. 2% of total body mass in all three species. Drawn from data in Bernal *et al*. (2003*a*).

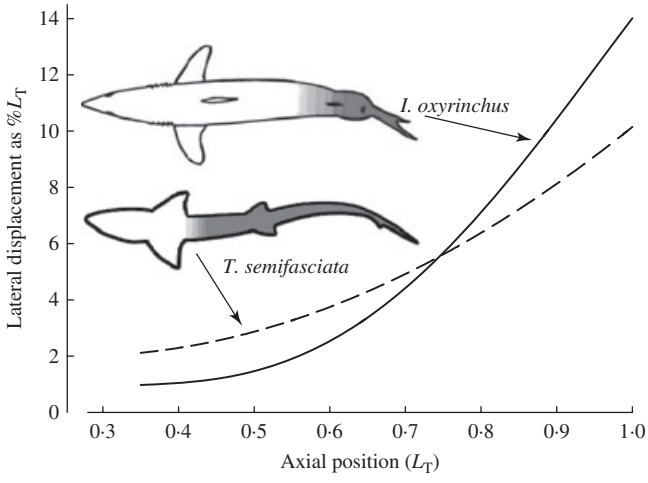

FIG. 10. The amplitude of the propulsive wave along the body in swimming *Isurus oxyrinchus* and *Triakis semifasciata.* Lateral displacement, expressed as a percentage of the total body length (L_T), is relatively low anteriorly in *I. oxyrinchus* but increases sharply in the caudal region, compared to *T. semifasciata.*

L_T, the displacement is three times greater in *T. semifasciata*, they are equivalent at 0·75 L_T, while at the tail tip the amplitude is *c*. 40% greater in *I. oxyrinchus* than in *T. semifasciata*. This is even more remarkable considering that in *I. oxyrinchus* most of the red muscle occurs anterior to 0·65 L_T (Fig. 9), whereas most of the lateral motion caused by this muscle occurs posterior to this point (Fig. 10). Thus, the red muscle functions as if it is physically uncoupled from local body curvature, *i.e.* from direct connections with adjacent skin, surrounding white muscle and backbone. The anatomy and physiology support this. A lubricative sheath between the loin of red muscle and the surrounding white muscle allows independent movement of the two tissues (Bernal *et al*., 2001*b*; Donley *et al*., 2005); red muscle shortening and local body curvature have a phase difference of 10–15% of a tail-beat cycle, with contractions at the mid-body being in phase with lateral motion in the caudal region (Donley *et al*., 2005). These features are illustrated in Fig. 11, which shows examples of the body midlines in a swimming *I. oxyrinchus* along with measured lateral displacements and red muscle strains. For example, shortening of red muscle at 0·4 L_T is coincident with lateral motion at about the leading edge of the caudal fin, while shortening of red muscle at 0·6 L_T is in phase with lateral motion of the tail tip. Another consequence of this uncoupling is that the propagation of the wave of deformation along the body is rapid, *c*. 2 L_T per tail beat, or twice as fast in *T. semifasciata*, giving a propulsive wavelength of 2 L_T, also twice the value as in *T. semifasciata.*

In vivo measurements of muscle activation and strain patterns in swimming *I. oxyrinchus* revealed similar trends to those in *T. semifasciata*, with the following notable differences (Donley *et al.,* 2005; Fig. 12). At both 0·4 and 0·6 L_T, red muscle strains were higher (±5·5 to ±8·7%) than in *T. semifasciata* (±3·9 to ±6.6%), although midline curvature was lower. Muscle activation occurs relatively late in lengthening, <2% of a cycle period in advance of peak length, at both 0·4 and 0·6 L_T, resulting in only very short periods of lengthening while active. Similar activation phase and duration were observed at 0·4 and 0·6 L_T.

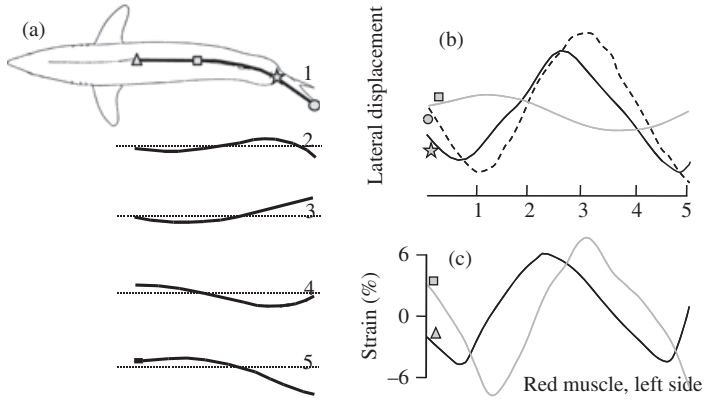

FIG. 11. Correlation between body kinematics and red muscle dynamics in a steady swimming *Isurus oxyrinchus*. (a) Dorsal midline traces from 0·4 total length, (L_T), to the tail tip (1·0 L_T) for selected time intervals through one complete tail-beat cycle. Numbers indicate points in time as the tail-beat cycle progresses; symbols indicate positions along the body (△, 0·4 L_T; □, 0·6 L_T, ☆, the leading edge of the caudal fin; ○, the tail tip). (b) Lateral displacement of the three posterior positions as a function of time for the tail-beat cycle shown in (a). (c) Red muscle strain for 0·4 L_T (——) and 0·6 L_T (——) on the left side of the body on the same time scale as (a). Redrawn from Donley *et al*. (2005) with permission from the Company of Biologists.

The effects of temperature on red muscle mechanics

An important technique that has been developed to measure force and length changes in cyclic contractions is the work loop (Syme, 2006). This provides a method to mimic *in vivo* muscle function that is particularly useful for locomotion where the muscle performs regular and cyclic contractions, such as in swimming. Briefly, an isolated sample of muscle fibres is maintained in a temperature-controlled saline

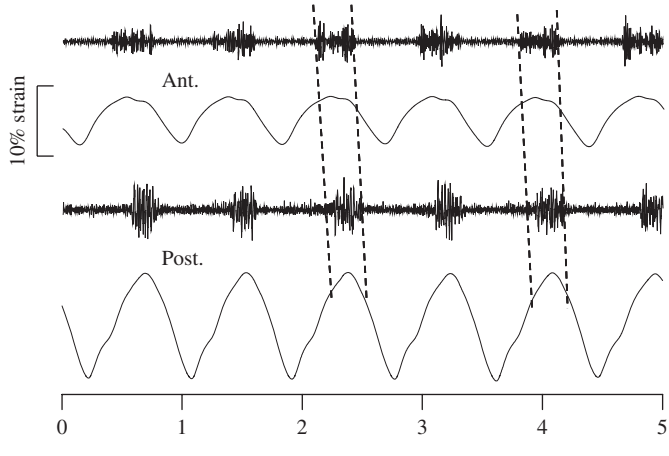

FIG. 12. Muscle activation and strain (sonomicrometry) recorded simultaneously over consecutive tail-beat cycles in anterior (Ant.) (0·4 total length, L_T) and posterior (Post.) (0·6 L_T) axial positions in an *Isurus oxyrinchus*. Here, the duration and phase of activation relative to strain are the same at both locations (– – – –). Redrawn from Donley *et al*. (2005) with permission from the Company of Biologists.

bath, tied by connective tissue at one end to a force transducer and at the other end to a displacement actuator. Typically, imposed displacement (muscle strain) is sinusoidal with frequency and amplitude of the actuator under computer control. Electrical activation is provided by a stimulator synchronized with the strain cycle by the computer. Each experiment consists of lengthening and shortening cycles with activation while force and length are continuously measured. Plots of force *v*. length yield the work loop, allowing work per cycle to be determined. The frequency, strain amplitude, and stimulus onset and duration are all important factors that determine how much net work is performed in one contraction cycle. Generally, work per cycle decreases as cycle frequency increases, because there is less time for the muscle to relax after the stimulus period, eventually the frequency is too great for any positive contractile work to be performed. Because power is the rate of doing work (work cycle^{-1} $\times$ cycles s^{-1} = Js^{-1} = W), net power may increase with frequency if the drop in work per cycle is less than the increase in frequency. The first application of the work-loop technique to shark muscle, including measurements of net work and heat output (Table I), involved both white and red fibres from *S. canicula* (Curtin & Woledge, 1993*a*, *b*). More recently, activation timing patterns for *T. semifasciata* and *I. oxyrinchus* recorded *in vivo* have been used to set parameters for *in vitro* work-loop experiments (Donley *et al*., 2007). Their results showed that the twitch properties of red muscle from anterior and posterior locations in each species were statistically indistinguishable, quite unlike the situation in many teleosts where axial variation in muscle contractile properties has been demonstrated (Syme, 2006). In addition, the stimulus conditions that produced maximum work and power (stimulus onset and duration) were also similar for both locations. These observations of muscle performance *in vitro* match with the patterns of muscle activation timing recorded *in vivo* [Figs 7(b) and 12].

The effect of temperature on red muscle power output in three species of sharks is shown in Fig. 13. In these plots, the work-loop cycle frequency mimics the tail-beat frequency, and therefore the swim speed of the fish. In the ectotherm *T. semifasciata* [Fig. 13(a)], power peaks near 0·5 Hz at 15° C (*c*. 0·3 L_T s^{-1}; Shadwick & Gemballa, 2006), but increases in magnitude and peaks near 1 Hz at 20° C (*c*. 0·6 L_T s^{-1}). Further increase in temperature led to a decline in power output. These results show that at typical swim speeds of 0·5–1·0 L_T s^{-1} red muscle in this species is operating near its optimum for power and efficiency, whereas >20° C, muscle performance is suboptimal (Donley *et al*., 2007). Temperature sensitivity is much more marked in *I. oxyrinchus* red muscle [Fig. 13(b)]. Here, maximum power output and its frequency are sharply increased from 25 to 28° C, but power output is so diminished at 15° C, that it is unlikely the fishes could swim at that muscle temperature. These results suggest that the muscle in the endothermic *I. oxyrinchus* is well adapted to function at the elevated temperatures it normally experiences (*i.e.* >20° C; Fig. 8), at the expense of potential for use at lower temperatures (Donley *et al*., 2007).

A similar result, but to a greater extreme, was obtained from work-loop experiments on red muscle from large *L. ditropis* obtained in Alaska [Fig. 13(c)]. In this species, power production was greatly enhanced up to at least 30° C, but was virtually zero below 20° C (Bernal *et al*., 2005). Interestingly, Alaskan *L. ditropis* spend much of their time in water temperatures of 5–10° C (Weng *et al*., 2005), at which their red muscle would be non-functional if it were to cool to ambient

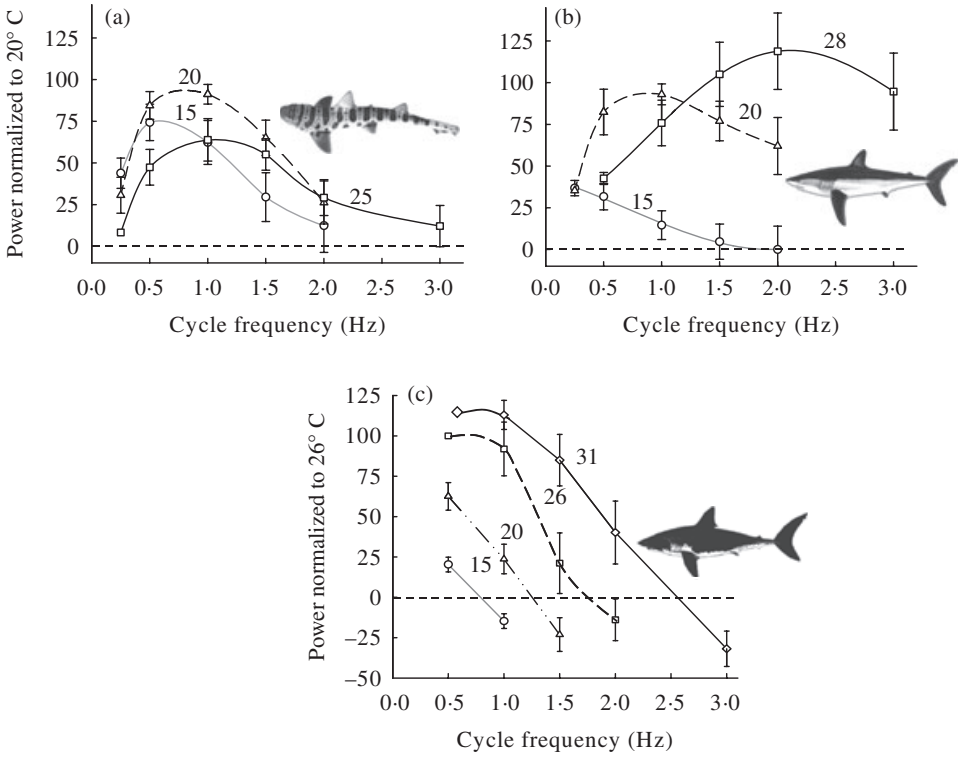

FIG. 13. Red muscle power output as a function of cycle frequency and temperature in (a) *Triakis semifasciata*, (b) *Isurus oxyrinchus* and (c) *Lamna ditropis*. Values of power are normalized to the maximum at 20° C for (a and b) and 26° C for (c). Cycle frequency axis is equivalent to tail-beat frequency, thus an index of swim speed. Data are from *in vitro* work-loop experiments on isolated muscle fibres (Bernal *et al*., 2005, with permission from Nature; Donley *et al*., 2007, with permission from the Company of Biologists).

temperature. Clearly, regionally endothermic lamnids have a requirement for elevated red muscle temperature that is provided by heat retention from their sustained swimming.

Alopias vulpinus*, the other warm-bodied shark*

The common thresher shark *Alopias vulpinus* (Bonnaterre 1788) has anteriorly focussed, internalized red muscle and elevated core body temperatures (Bernal & Sepulveda, 2005; Sepulveda *et al*., 2005). This seems even more remarkable considering that the other species of Alopiidae, which have very similar body morphology, are ectothermic and have only superficial red muscle. A recent study in which muscle activation and strain were measured in swimming *A. vulpinus* demonstrated an uncoupling of the red muscle from local bending and surrounding white muscle, just as in *I. oxyrinchus*, but without the stiff-bodied swimming mode (Bernal *et al*., 2010). Details of the myoseptal anatomy in *A. vulpinus* and the temperature sensitivity of its red muscle, when available, should provide interesting insight into the phenomenon of regional endothermy and swimming mechanics.

UNSTEADY SWIMMING: FAST-STARTS AND BURSTS

Unlike steady aerobic swimming, unsteady fast-starts and burst sprints are transient, high-acceleration manoeuvres initiated either at rest or during steady swimming, and powered by fast white muscle. This highly specialized behaviour is critically important for capturing prey and avoiding predators in a variety of fishes. Nearly all studies of the neurobiology, kinematics or muscle activity involved in unsteady swimming have been conducted on teleosts, and have generated a good understanding of this phenomenon and its evolutionary origins (Weihs, 1973; Eaton *et al*., 1977; Webb, 1978; Nissanov & Eaton, 1989; Eaton & Emberley, 1991; Jayne & Lauder, 1993; Domenici & Blake, 1997; Wakeling & Johnston, 1998, 1999; Wakeling *et al*., 1999; Wakeling, 2001; Tytell & Lauder, 2002).

FAST-STARTS

Weihs (1973) first categorized fast-starts into three stages of motion: a preparatory bend to one side of the body (stage 1), a propulsive kick (stage 2) and a variable stage where the fish may glide to a halt or continue to swim (stage 3). Subsequently, the transitions between stages have been more specifically defined EMG (Jayne & Lauder, 1993), onset of forward propulsion (Foreman & Eaton, 1993) and change in turning direction (Kasapi *et al*., 1993).

A clear feature of fast-starts is that a wave of strong contraction is propagated rapidly along the white fibres of one side of the body to initiate the C-bend away from the stimulus, characteristic of stage 1. In a few cases where this has been quantified, the muscle activation, measured as EMG activity, is near-synchronous (within a few ms) along the entire side contralateral to the stimulus, implicating the involvement of a fast neuronal conduction system separate from what controls undulatory swimming. Indeed, it is well accepted that fast-starts in fishes and aquatic amphibians are initiated by large paired reticulospinal neurons called Mauthner cells (Wilson, 1959; Eaton *et al*., 1981; Korn & Faber, 2005) or their homologues (Kohashi & Oda, 2008). The axons of these cells extend the length of the spinal cord, and their interaction with spinal interneurons transduces a stimulus on one side of the head into a rapid and strong activation of motor neurons on the contralateral side, initiating muscle contraction to power the escape response, even if the fish is already swimming forward (Fetcho & Faber, 1988; Fetcho, 1991; Eaton *et al*., 1995; Korn & Faber, 2005). Stage 2 appears to be based on a propulsive wave of muscle contraction, similar to what is seen in burst swimming (Westneat *et al*., 1998; Ellerby & Altringham, 2001).

The most basal extant lineage in which Mauthner cells and startle behaviour occurs is the Petromyzontidae (Rovainen, 1978, 1983; McClellan & Grillner, 1983). Comparative analyses suggest that startle responses are evolutionarily conserved, whereby the fast-start escape response in teleosts is derived from a primitive head withdrawal response, as seen in petromyzontids, which involves bilateral muscle activation (Hale *et al*., 2002). This hypothesis is supported by evidence that some basal actinopterygians (*Amia* and *Polypterus*) exhibit strong bilateral muscle activation during fast-starts (Tytell & Lauder, 2002), while in more derived teleosts such as trout *Oncorhynchus mykiss* (Walbaum 1792) and *C. auratus* activation on the ipsilateral side is absent or only weak. Mauthner cells have been described in embryos and small pups of two squaloid sharks (*S. acanthias* and *Dalatias licha*; Bonnaterre

1788), but not in adults nor in any stages of *S. canicula* (Bone, 1977). Therefore, the role of a rapid conduction neuronal system to control escape manoeuvres in sharks has not been confirmed. To date, only one study has examined fast-start kinematics in any elasmobranch (Domenici *et al*., 2004) and no measurements of muscle activation patterns are yet available. Working with the spotted spiny dogfish *Squalus suckleyi* (Girard 1855), Domenici *et al*. (2004) showed that escape responses were relatively slow compared to those of teleosts, but had tight turning radii, reflecting their low locomotor performance and high flexibility. Further, they suggested that the escape behaviour may consist of two types of response, distinguished by two distinct rates of turning of the anterior part of the body.

To further investigate this phenomenon in sharks, muscle activation was measured by electromyography in *T. semifasciata* during induced escape responses. Experiments were conducted on six specimens (mean ± S.D. $L_T = 79{\cdot}0 \pm 8{\cdot}7$ cm), at the Scripps Institution of Oceanography, San Diego, U.S.A. Stainless steel wire electrodes were implanted in white muscle at three longitudinal positions (0·3, 0·5 and 0·7 L_T) entering near the dorsal midline to a depth of that approximated the centre of the dorsal posterior cone of muscle, under mild benzocaine anaesthesia. Electrodes were marked with indelible ink at the point of entry so their position could be verified at the end of the experiments. After a recovery period 24 h or longer in a 3 m diameter tank at 18–20° C, escape responses were elicited by dropping a 1 kg weight. Simultaneously, digital video images were recorded at 60 Hz and amplified EMG signals were recorded at 2 kHz. Digital image analysis was used to calculate midline points in video sequences, midline curvatures were calculated and used as an index of muscle strain, and these data were synchronized with EMG signals by a sequence of LED pulses.

The general form of the escape response is a tight C-bend of the body, [Fig. 14(a)], similar to what has been described for many fishes, including sharks (Domenici *et al*., 2004). The kinematics of the C-turn can be described by the stage 1 turning rate and final angular displacement. Turning angle is measured as the rotation of a line drawn through the snout and the body centre of mass at 0·33 L_T. The stage 1 bending angle typically exceeded 100°, and in the strongest responses the curvature was great enough that the head would touch the tail. In some instances, the C-start was followed by a stage 2 propulsive stroke [Fig. 14(b)]. The lack of stage 2 in many cases may have been influenced by the confined space in the experimental tank. Responses could be broadly grouped into fast (stage 1 duration <260 ms) and slow (stage 1 duration up to 500 ms) categories, as was seen for *S. suckleyi* (Domenici *et al*., 2004). These coincided with mean head turning rates of 330–400 and 520–920° s^{-1}, respectively [Figs 14(c), (d) and 15].

Sequential EMG recordings revealed that fast-starts in sharks, as in teleosts, are powered by near-simultaneous activation of lateral white muscle along the body, with transit times of the activation between the most anterior and posterior recording positions being typically <10 ms, *i.e.* the activation wave speed is >40 L_T s^{-1}(Fig. 16). Most interestingly, bilateral muscle activation was observed in all but the weakest fast-starts (Fig. 16). Muscle activation occurred only during the initial part of the C-bend; in contrast, activation of white fibres during fast swimming is less intense and accompanied by a delay of 200–300 ms from 0·3 to 0·7 L_T, indicating that the activation travels at only 1–2 L_T s^{-1} along the body. These results suggest that

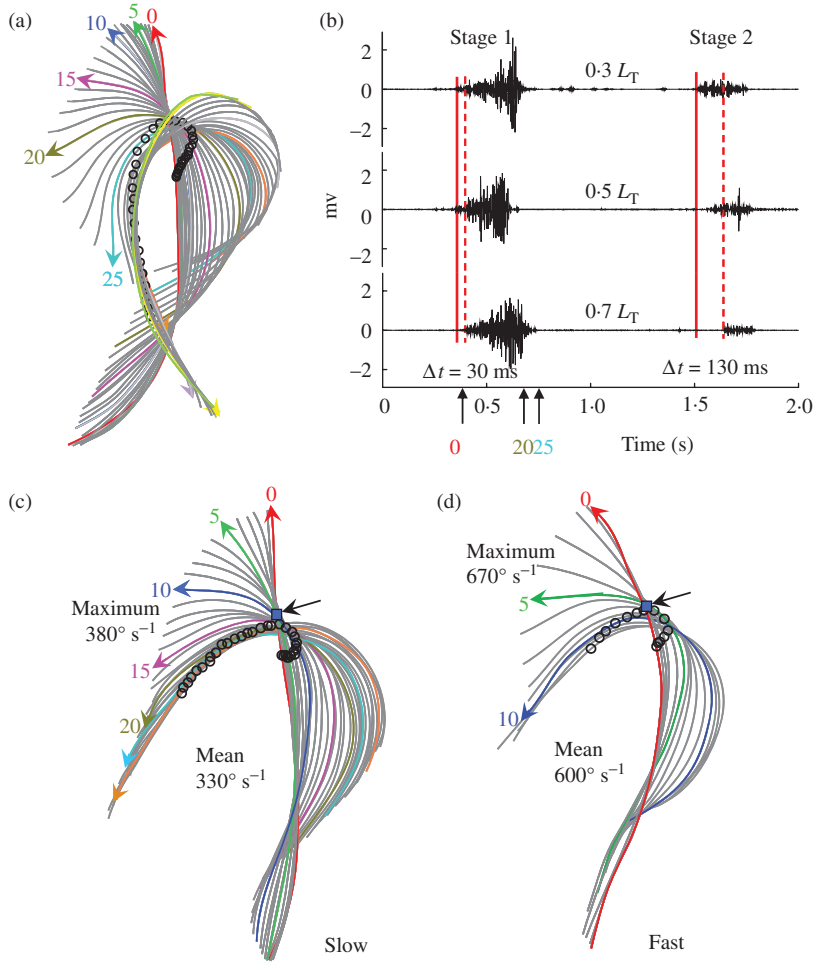

FIG. 14. (a) Numbered sequence of body midlines from a fast-start escape response of *Triakis semifasciata* filmed at 16·7 ms intervals. ○, 0·33 total length (L_T) for each frame, representing the centre of mass of the straight body. (b) Muscle activation measured at three locations on the left side of the body, showing a rapid activation for stage 1, followed by slower activation of stage 2 propulsive stroke. (c and d) Examples of slow- and fast-escape responses (16·7 ms intervals), indicating maximum and mean turning rates in degrees per second during stage 1. The ■ (→), marks the apparent centre of rotation during initial phase, at *c*. 0·24 L_T.

escape responses are controlled by a faster muscle activation system than is used for fast undulatory swimming.

What is the effect of bilateral muscle activation in a C-start? One possibility is that by activating muscles on both sides the body is stiffened and the propulsive wave speed is increased. In addition, bending of the tail region away from the direction of the C is often observed (Fig. 17), indicating that muscle in the posterior body is shortening to flex the tail, perhaps to resist the torque of the turning head. Two examples of this in which muscle length changes have been calculated from body curvature are shown in Fig. 18.

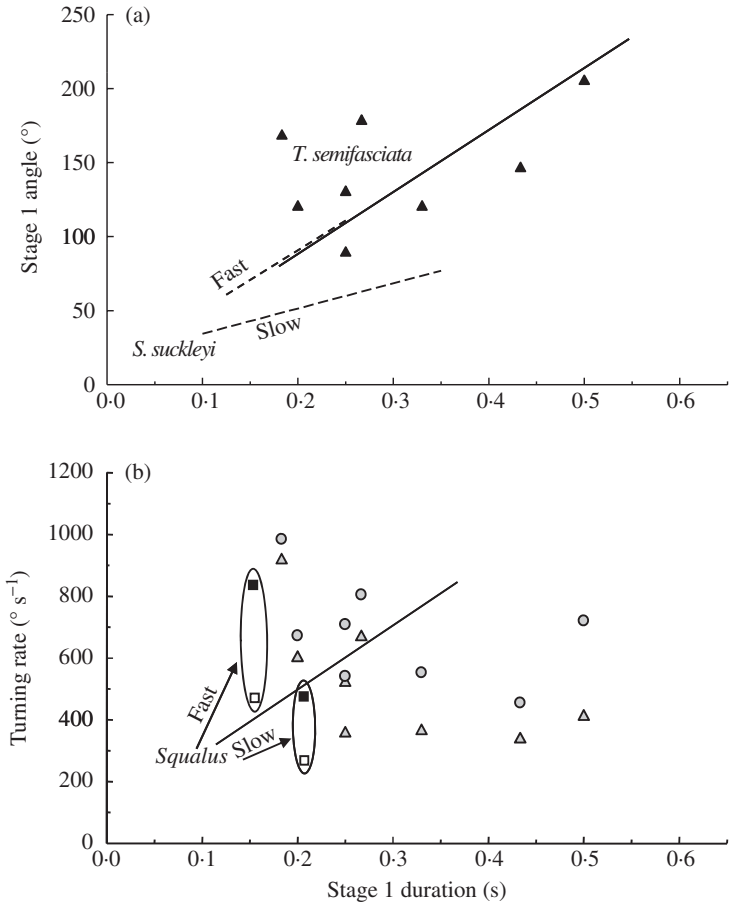

FIG. 15. Stage 1 angle *v*. stage 1 duration for fast-starts in *Triakis semifasciata* (▲). ___, delineates the upper and lower group of data as fast and slow responses, respectively. For comparison, - - - show results for fast-starts in *Squalus suckleyi* tested at 12° C (Domenici *et al*., 2004). (b) *Triakis semifasciata* mean head turning rate during entire stage 1 (△), and maximum turning rate over five video fields (○). Range of head turning rates for *S. suckleyi* slow and fast turns are also shown (maximum; ■) and (minimum; □) (data from Domenici *et al*., 2004).

BURST SWIMMING

Unlike fast-starts, burst sprints are powered by brief but symmetrical contractions of the lateral musculature, similar to steady swimming but at higher tail-beat frequencies. Experimentally, this is a difficult activity to study, so there are limited data on any fish to date. It seems likely that burst speeds will vary linearly with tail-beat frequency, as has been shown in some teleosts (Bainbridge, 1958; Fierstine & Walters, 1968), but increased tail amplitudes may also be employed, driven by higher muscle shortening strains (Ellerby & Altringham, 2001). In a water tunnel, *M. henlei* swam to 4 L_T s^{-1} using a tail-beat frequency of 5 Hz (Hunter & Zweifel, 1971) and the blacktip reef shark *Carcharhinus melanopterus* (Quoy & Gaimard 1824) made bursts up to 4 L_T s^{-1} at 8 Hz in a large aquarium (Webb & Keyes, 1982).

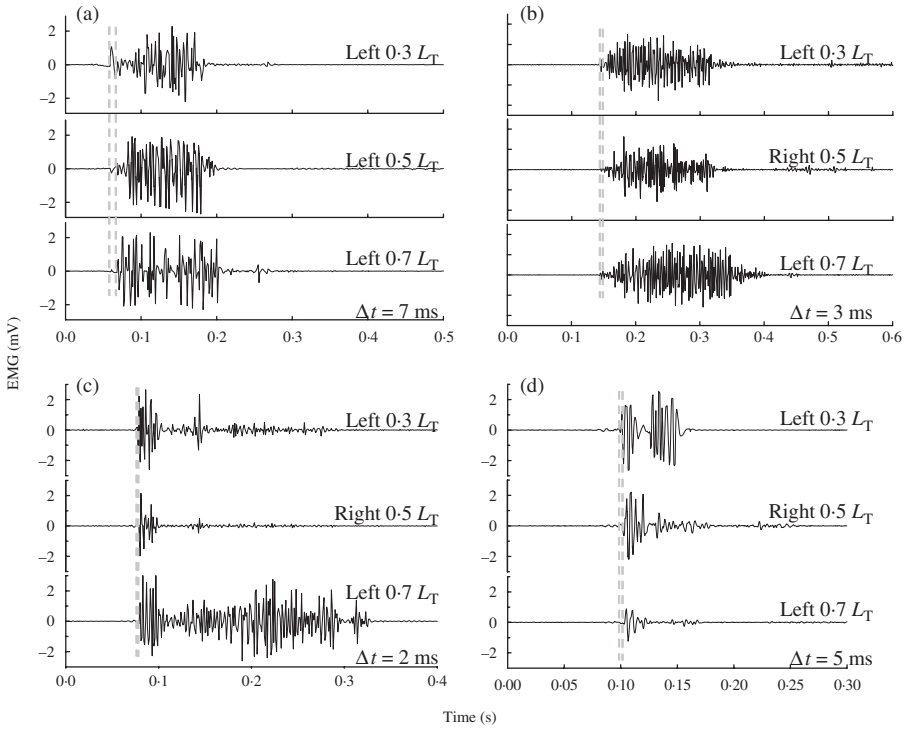

FIG. 16. (a) Muscle activation patterns in fast-starts by *Triakis semifasciata,* showing the very fast axial propagation during stage 1. (a) Recordings at three sites along left side; fish turns to the left. (b–d) Examples of bilateral activation in stage 1, all turns to left (L_T, total length).

Some measurements of natural burst speeds have been obtained in field studies. Using a speed-sensing transmitter on seven 1·5–1·8 m lemon sharks *Negaprion brevirostris* (Poey 1868), researchers reported an average burst speed of 1·72 m s^{-1} (0·97 L_T s^{-1}) with an average duration of 7 s and a maximum burst speed of 5 m s^{-1} (3·1$L_T s^{-1}$) for 2 s (Sundström *et al*., 2001). The highest burst speeds reported are for *I. oxyrinchus*; calculations from ultrasonic transmitters on 1·2–1·4 m sharks were up to 8–9 m s^{-1} (6·4–6·6 L_T s^{-1}) (Klimley *et al*., 2002).

Other estimates of burst speeds come from observations of sharks jumping out of the water. For example, from simple physics of projectile motion, Brunnschweiler (2005) calculated the water escape velocity for jumps by 1·6 m blacktip sharks *Carcharhinus limbatus* (Müller & Henle 1839) based on video records, and found the average to be 6·3 m s^{-1} (3·9 L_T s^{-1}). Likewise observations here of *I. oxyrinchus* (*c*. 1–1·4 m long) jumping while attacking bait yielded sprint speed estimates of 5–6 m s^{-1} (3·6–6.0 L_T s^{-1}) (R. Shadwick, pers. obs.).

SWIMMING AND MIGRATION

The complex neuromuscular systems in sharks underlie the ability of many species to perform efficient, high-performance locomotion. Sharks exhibit an extensive

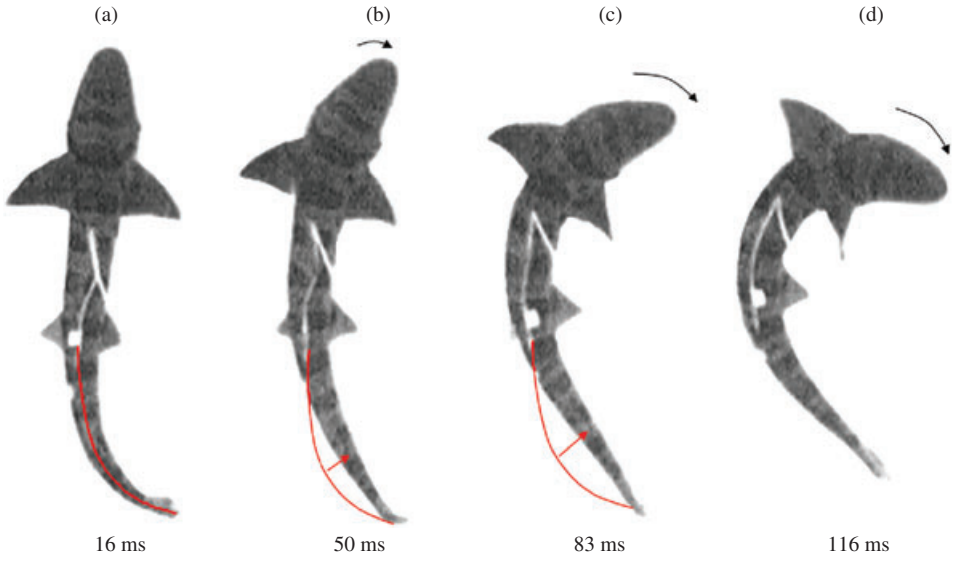

FIG. 17. *Triakis semifasciata* fast-start showing how flexion on the posterior left side (——, ⟶) opposes the direction of the head turn (⟶), indicating that muscle activation occurs on both sides at the beginning of stage 1. (a–d) Images from a video sequence with times from initiation of the fast-start shown below each.

repertoire of swimming behaviours from long-distance migrations to acrobatic trajectories during predator and prey interactions. Such locomotor capacities enable sharks to play a major role in diverse ecosystems as apex predators at multiple trophic levels. Advances in tag technology have enabled the analysis of shark distribution and large-scale movement, thereby revealing new insights into the physiological ecology of habitat selection, migratory behaviour and life history (Sims & Quayle, 1998; Sims, 1999; Boustany *et al*., 2002; Bonfil *et al*., 2005; Weng *et al*., 2005, 2007; Meyer *et al*., 2009; Skomal *et al*., 2009; Cartamil *et al*., 2010*a*, 2011; Jorgensen *et al*., 2010; Block *et al*., 2011; Campana *et al*., 2011; Hammerschlag *et al*., 2011; Papastamatiou *et al*., 2011; Saunders *et al*., 2011). In addition, high-resolution archival tags and acoustic telemetry provide information on fine-scale movement during diving, foraging and mating (Sepulveda *et al*., 2004; Gleiss *et al*., 2009; Barnett *et al*., 2010; Cartamil *et al*., 2010*b*; Whitney *et al*., 2010; Gleiss *et al*., 2011*a*; Nakamura *et al*., 2011). As has been shown in other study taxa (Block, 2005; Rutz & Hays, 2009; Ropert-Coudert *et al*., 2010), the recent advent and proliferation of biologging techniques across temporal and spatial scales has a strong potential to enhance understanding of shark biology in their natural environment.

Satellite tag studies have revealed extensive migratory abilities in many shark species that exhibit a lamniform-like body shape, some of which include *C. carcharias* (Bonfil *et al*., 2005), *L. ditropis* (Weng *et al*., 2005), *P. glauca* (da Silva *et al*., 2010), basking sharks *Cetorhinus maximus* (Gunnerus 1765) (Gore *et al*., 2008; Skomal *et al*., 2009) and *R. typus* (Brunnschweiler *et al*., 2009). These taxa are capable of trans-oceanic and trans-equatorial migrations that are typically in excess of several thousand km. The most far-reaching migrations are exhibited by lamnids,

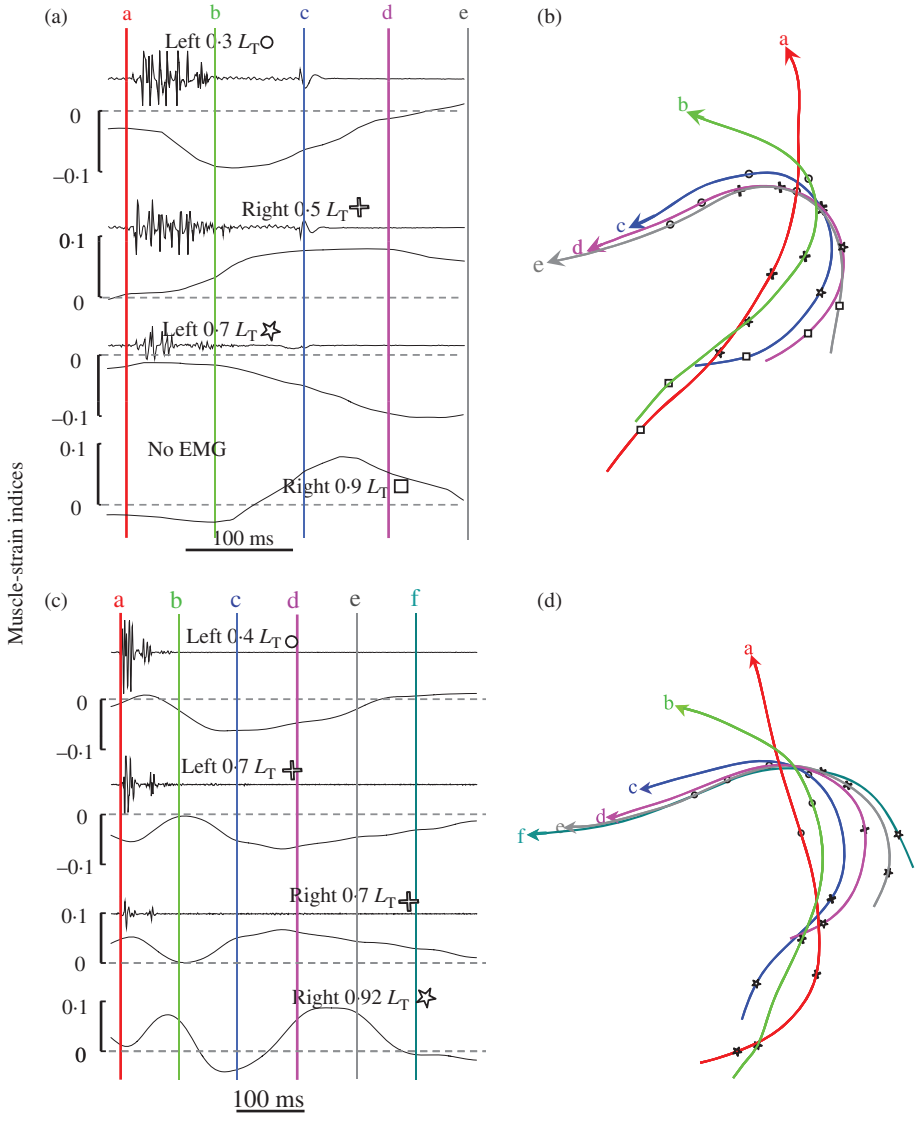

FIG. 18. Temporal relation between muscle activation and muscle shortening along the body in two fast-starts of *Triakis semifasciata*. (a and c) Midline curvature at four axial positions is used as an index of muscle strain. Positive values indicate convex curvature and muscle lengthening, negative values indicate concave curvature and muscle shortening and zero represents no curvature. Electromyograph (EMG) muscle activation traces are also shown for each location except the most posterior right side where there were no electrodes. (b and d) Coloured midline traces from a video sequence which correspond to coloured time lines on (a) and (c), respectively. Markers along the midlines represent positions of muscle-strain index plots (○, 0·3 total length L_T; ✚, 0·5 L_T; ☆, 0·7 L_T; □, 0·9 L_T in (a)) (○, 0·4 L_T; ✚, 0·7 L_T; ☆, 0·92 L_T in (c)). Activation occurs primarily in the early portion of the C-bend, ipsilateral muscle is actively shortening, but contralateral muscle in mid-body is being lengthened while active. Muscle shortening on right side at 0·9–0·92 L_T occurs while the body is turning to the left, causing the initial contralateral flexion in the posterior region.

with the longest record to date being a *C. carcharias* that undertook a round-trip excursion of >20 000 km across the Indian Ocean (Bonfil *et al*., 2005). This extreme migratory capacity is undoubtedly facilitated by the specialized physiological systems of lamnids that increase power output and enhance swimming performance (Shadwick, 2005). Endothermic muscle combined with cold-water cardiac adaptations has expanded ecological niche and broadened home range for some of these species, such as *L. ditropis* (Weng *et al*., 2005). Medium to large-bodied sharks that lack regionalized endothermy still have the capacity for large-scale migrations (Brunnschweiler *et al*., 2009; Skomal *et al*., 2009), but these species are disproportionally represented among satellite tag studies (Hammerschlag *et al*., 2011). Although long-distance migration may not require large body size (Aarestrup *et al*., 2009), larger species may still benefit from a lower cost of transport (Schmidt-Nielsen, 1984) and greater thermal inertia that can help retain heat from ectothermic muscle (Bostrom & Jones, 2007) and therefore increase power output during swimming.

Many archival tags include a compound suite of sensors including a pressure transducer, a paddle-wheel or hydrophone speedometer and a tri-axial accelerometer and magnetometer (Burgess *et al*., 1998; Johnson & Tyack, 2003; Muramoto *et al*., 2004). Together, these sensors can provide an estimate of the animal's body orientation (Johnson & Tyack, 2003) and, if additional information is available such as geolocation fixes of surfacing events or data on water current direction and magnitude, a three-dimensional reconstruction of its underwater trajectory (Ware *et al*., 2006, 2010; Shiomi *et al*., 2008). Transient, high-frequency signals detected by the accelerometer may reflect swimming strokes executed by the animal and thus allow swimming gaits and movement strategies to be analysed and compared among species (Gleiss *et al*., 2011*b*). Furthermore, researchers have used the acceleration signals measured by electronic tags to determine a shark's behavioural state (*i.e.* fast-start *v*. steady swimming), and to estimate relative rates of energy expenditure (Gleiss *et al*., 2009, 2010, 2011*c*).

Speed is a prime determinant of energy expenditure during locomotion and a key metric of swimming performance in fishes. Biologging techniques to measure speed in free-ranging sharks have included a propeller (Nakamura *et al*., 2011) and acoustic telemetry (Sundström & Gruber, 1998; Lowe & Goldman, 2001; Lowe, 2002). When tagging is not possible, however, alternative methods using photogrammetry (Lacey *et al*., 2010), speed matching with an adjacent research vessel (Sims & Quayle, 1998; Sims, 1999, 2000) and various geometric calculations (Harden Jones, 1973; Weihs *et al*., 1981; Brunnschweiler, 2005) have been used to estimate shark speeds at the sea surface. All measurements for free-ranging sharks indicate a relatively low speed during steady swimming that is generally <2 m s^{-1}. Klimley *et al*. (2002) found that lamnids (*Isurus* and *Carcharodon*) maintained higher speeds than an ectothermic carcharhinid species (*P. glauca*).

Putting field measurements in the context of laboratory results, it is noteworthy that sharks swimming in water tunnels typically prefer speeds of <1 m s^{-1}, and maximal aerobic swim velocities are generally observed to be well below 2 m s^{-1} (Hunter & Zweifel, 1971; Graham *et al*., 1990; Lowe, 1996; Donley & Shadwick, 2003; Donley *et al*., 2005; Sepulveda *et al*., 2007. Thus, it is likely that the speed at which cost of transport is minimized is on the order of 1 m s^{-1}, or less, but perhaps higher in the Lamnidae. Although more research is needed that focuses on the fine-scale movement and swimming kinematics in sharks, such a low choice of

swimming speed may be a universal phenomenon among all swimming animals (Sato *et al*., 2007, 2010; Watanabe *et al*., 2010), as predicted from the intrinsic contractile properties of muscle (Hill, 1950). By choosing a low swimming speed, as shown from a large data set of air breathing divers, swimming animals will minimize transport costs associated with the muscle power output required to overcome drag and buoyant forces (Sato *et al*., 2010; Watanabe *et al*., 2010; Gleiss *et al*., 2011*a*).

FUTURE DIRECTIONS

One aspect that is poorly understood is how white muscle powers burst swimming, particularly in free-ranging animals, and this is an area which is hoped to gain attention in future work. As yet, there are no direct measurements of muscle activation or contraction dynamics in white muscle during maximal activity, except for the data presented here for fast-starts. While work on captive animals may be logistically easier, collecting this type of data from unrestrained sharks or tethered sharks in the open ocean would be much more reliable. Advances in electronic tag design will probably provide the means to make these measurements in the near future, and should allow the range of species studied to be expanded. This could permit estimates of muscle power to be made, and exploration of the reasons why routine cruising speeds in sharks seem typically lower than in teleosts.

The energetic cost of swimming needs to be investigated. Limited data on water-tunnel studies of steady swimming are available, but are not extensive. Cost of transport is unknown in pelagic species and, considering the extensive migrations of some species, it would be interesting to know if their cruising speeds of <1 m s^{-1} reflect the minimum cost of transport. It would also be interesting to know how the aerobic scope of sharks varies among body types and in comparison with teleosts, particularly the comparison of lamnids with tunas. Assuming the lamnids are the most athletic sharks, it would be appealing in terms of evolutionary convergence to examine how hydrodynamic thrust is produced from the lunate tails and how their white muscle power potential compares with tunas.

The recent ability to transmit accelerometer data acoustically *via* the Ocean Tracking Network (http://otncanada.org/) has the potential to revolutionize the study of fish energetics and behaviour. By taking the norm of acceleration measured along three orthogonal axes, researchers have just begun to estimate energy expenditure during steady swimming in free-ranging fishes. Because swimming tail-beat frequency is expected to vary with body size, spectrograms of accelerometer signals could be used to determine fish body size. Such an approach would be particularly effective for examining growth trajectories of young sharks in the open ocean. If accelerometers are combined with magnetometers, a three-dimensional reconstruction of the animal's body orientation can be obtained as well. Field studies still benefit from laboratory procedures, if size permits, so that tag sensors can be calibrated and properly interpreted. Future efforts should aim to integrate archival tags with the acoustic telemetry in order to open new areas of research in understudied and threatened species.

The authors would like to acknowledge support for this work from NSERC and NSF.

References

Aarestrup, K., Okland, F., Hansen, M. M., Righton, D., Gargan, P., Castonguay, M., Bernatchez, L., Howey, P., Sparholt, H., Pedersen, M. I. & McKinley, R. S. (2009). Oceanic spawning migration of the european eel (*Anguilla anguilla*). *Science* **325**, 1660.

Alexander, R. M. (1965). Lift produced by the heterocercal tails of *Selachii*. *Journal of Experimental Biology* **43**, 131–138.

Alexander, R. M. (1969). Orientation of muscle fibers in myomeres of fishes. *Journal of the Marine Biological Association of the United Kingdom* **49**, 263–290.

Altringham, J. D. & Johnston, I. A. (1982*a*). The mechanical properties of skinned fast and slow fibers isolated from fish myotomal muscle. *Biophysical Journal* **37**, A361 .

Altringham, J. D. & Johnston, I. A. (1982*b*). The PCA-tension and force-velocity characteristics of skinned fibers isolated from fish fast and slow muscles. *Journal of Physiology-London* **333**, 421–449.

Bainbridge, R. (1958). The speed of swimming of fish as related to size and to the frequency and amplitude of the tail beat. *Journal of Experimental Biology* **35**, 109–133.

Barnett, A., Abrantes, K. G., Stevens, J. D., Bruce, B. D. & Semmens, J. M. (2010). Fine-scale movements of the broadnose sevengill shark and its main prey, the gummy shark. *PLoS ONE* **5**, e15464.

Bernal, D. & Sepulveda, C. A. (2005). Evidence for temperature elevation in the aerobic swimming musculature of the common thresher shark, *Alopias vulpinus*. *Copeia* **2005**, 146–151.

Bernal, D., Sepulveda, C. & Graham, J. B. (2001*a*). Water-tunnel studies of heat balance in swimming mako sharks. *Journal of Experimental Biology* **204**, 4043–4054.

Bernal, D., Dickson, K. A., Shadwick, R. E. & Graham, J. B. (2001*b*). Review: analysis of the evolutionary convergence for high performance swimming in lamnid sharks and tunas. *Comparative Biochemistry and Physiology A* **129**, 695–726.

Bernal, D., Sepulveda, C., Mathieu-Costello, O. & Graham, J. B. (2003*a*). Comparative studies of high performance swimming in sharks. I. Red muscle morphometrics, vascularization and ultrastructure. *Journal of Experimental Biology* **206**, 2831–2843.

Bernal, D., Smith, D., Lopez, G., Weitz, D., Grimminger, T., Dickson, K. & Graham, J. B. (2003*b*). Comparative studies of high performance swimming in sharks II. Metabolic biochemistry of locomotor and myocardial muscle in endothermic and ectothermic sharks. *Journal of Experimental Biology* **206**, 2845–2857.

Bernal, D., Donley, J. M., Shadwick, R. E. & Syme, D. A. (2005). Mammal-like muscles power swimming in a cold-water shark. *Nature* **437**, 1349–1352.

Bernal, D., Donley, J. M., McGillivray, D. G., Aalbers, S. A., Syme, D. A. & Sepulveda, C. (2010). Function of the medial red muscle during sustained swimming in common thresher sharks: contrast and convergence with thunniform swimmers. *Comparative Biochemistry and Physiology A* **155**, 454–463.

Block, B. A. (2005). Physiological ecology in the 21st century: advancements in biologging science. *Integrative and Comparative Biology* **45**, 305–320.

Block, B. A., Finnerty, J. R., Stewart, A. F. R. & Kidd, J. (1993). Evolution of endothermy in fish: mapping physiological traits on a molecular phylogeny. *Science* **260**, 210–214.

Block, B. A., Jonsen, I. D., Jorgensen, S. J., Winship, A. J., Shaffer, S. A., Bograd, S. J., Hazen, E. L., Foley, D. G., Breed, G. A., Harrison, A. L., Ganong, J. E., Swithenbank, A., Castleton, M., Dewar, H., Mate, B. R., Shillinger, G. L., Schaefer, K. M., Benson, S. R., Weise, M. J., Henry, R. W. & Costa, D. P. (2011). Tracking apex marine predator movements in a dynamic ocean. *Nature* **475**, 86–90.

Bone, Q. (1966). On the function of the two types of myotomal muscle fibre in elasmobranch fish. *Journal of the Marine Biological Association of the United Kingdom* **46**, 321–349.

Bone, Q. (1977). Mauthner neurons in elasmobranchs. *Journal of the Marine Biological Association of the United Kingdom* **57**, 253–259.

Bone, Q. (1978). Locomotor muscle. In *Fish Physiology,* Vol. VII (Hoar, W. S. & Randall, D. J., eds), pp. 361–424. San Diego, CA: Academic Press.

Bone, Q. (1989). Muscles and locomotion. In *Physiology of Elasmobranch Fishes* (Shuttleworth, T. J., ed.), pp. 99–141. Berlin: Springer-Verlag.

Bone, Q. & Chubb, A. D. (1978). The histochemical demonstration of myofibrillar ATPase in elasmobranch. *Journal of Histochemistry and Cytochemistry* **10**, 489–494.
Bone, Q., Johnston, I. A., Pulsford, A. & Ryan, K. P. (1986). Contractile properties and ultrastructure of 3 types of muscle fiber in the dogfish myotome. *Journal of Muscle Research and Cell Motility* **7**, 47–56.
Bonfil, R., Meyer, M., Scholl, M. C., Johnson, R., O'Brien, S., Oosthuizen, H., Swanson, S., Kotze, D. & Paterson, M. (2005). Transoceanic migration, spatial dynamics, and population linkages of white sharks. *Science* **310**, 100–103.
Bostrom, B. L. & Jones, D. R. (2007). Exercise warms adult leatherback turtles. *Comparative Biochemistry and Physiology A* **147**, 323–331.
Boustany, A. M., Davis, S. F., Pyle, P., Anderson, S. D., Le Boeuf, B. J. & Block, B. A. (2002). Satellite tagging – expanded niche for white sharks. *Nature* **415**, 35–36.
Breder, C. M. (1926). The locomotion of fishes. *Zoologica* **4**, 159–297.
Brunnschweiler, J. M. (2005). Water-escape velocities in jumping blacktip sharks. *Journal of the Royal Society Interface* **2**, 389–391.
Brunnschweiler, J. M., Baensch, H., Pierce, S. J. & Sims, D. W. (2009). Deep-diving behaviour of a whale shark *Rhincodon typus* during long-distance movement in the western Indian Ocean. *Journal of Fish Biology* **74**, 706–714.
Burgess, W. C., Tyack, P. L., Le Boeuf, B. J. & Costa, D. P. (1998). A programmable acoustic recording tag and first results from free-ranging northern elephant seals. *Deep-Sea Research Part II in Oceanography* **45**, 1327–1351.
Campana, S. E., Dorey, A., Fowler, M., Joyce, W., Wang, Z., Wright, D. & Yashayaev, I. (2011). Migration pathways, behavioural thermoregulation and overwintering grounds of blue sharks in the northwest Atlantic. *PLoS ONE* **6**, e16854.
Carey, F. G., Casey, J. G., Pratt, H. L., Urquhart, D. & McCosker, J. E. (1985). Temperature, heat production and heat exchange in lamnid sharks. *Memoirs of the Southern California Academy of Sciences* **9**, 92–108.
Cartamil, D., Wegner, N. C., Kacev, D., Ben-aderet, N., Kohin, S. & Graham, J. B. (2010*a*). Movement patterns and nursery habitat of juvenile thresher sharks *Alopias vulpinus* in the Southern California Bight. *Marine Ecology Progress Series* **404**, 249–258.
Cartamil, D., Wegner, N. C., Aalbers, S., Sepulveda, C. A., Baquero, A. & Graham, J. B. (2010*b*). Diel movement patterns and habitat preferences of the common thresher shark (*Alopias vulpinus*) in the Southern California Bight. *Marine and Freshwater Research* **61**, 596–604.
Cartamil, D. P., Sepulveda, C. A., Wegner, N. C., Aalbers, S. A., Baquero, A. & Graham, J. B. (2011). Archival tagging of subadult and adult common thresher sharks (*Alopias vulpinus*) off the coast of southern California. *Marine Biology* **158**, 935–944.
Coughlin, D. J. (2002). Aerobic muscle function during steady swimming in fish. *Fish and Fisheries* **3**, 63–78.
Curtin, N. A. & Woledge, R. (1988). Power output and force-velocity relationship of live fibres from white myotomal muscle of the dogfish, *Scyliorhinus canicula*. *Journal of Experimental Biology* **140**, 187–197.
Curtin, N. A. & Woledge, R. C. (1993*a*). Efficiency of energy conservation during sinusoidal movement of white muscle fibers from the dogfish *Scyliorhinus canicula*. *Journal of Experimental Biology* **183**, 137–147.
Curtin, N. A. & Woledge, R. C. (1993*b*). Energetic propoerties of the red muscle fibers isolated from dogfish *Scyliorhinus canicula*. *Journal of Physiology (London)* **459**, P7.
Dickson, K. A., Gregorio, M. O., Gruber, S. J., Loefler, K. L., Tran, M. & Terrell, C. (1993). Biochemical indexes of aerobic and anaerobic capacity in muscle tissues of California elasmobranch fishes differing in typical activity level. *Marine Biology* **117**, 185–193.
Domenici, P. & Blake, R. W. (1997). The kinematics and performance of fish fast-start swimming. *Journal of Experimental Biology* **200**, 1165–1178.
Domenici, P., Standen, E. M. & Levine, R. P. (2004). Escape manoeuvres in the spiny dogfish (*Squalus acanthias*). *Journal of Experimental Biology* **207**, 2339–2349.
Donley, J. M. & Shadwick, R. E. (2003). Steady swimming muscle dynamics in the leopard shark *Triakis semifasciata*. *Journal of Experimental Biology* **206**, 1117–1126.

Donley, J. M., Sepulveda, C. A., Konstantinidis, P., Gemballa, S. & Shadwick, R. E. (2004). Convergent evolution in mechanical design of lamnid sharks and tunas. *Nature* **429**, 61–65.

Donley, J. A., Shadwick, R. E., Sepulveda, C. A., Konstantinidis, P. & Gemballa, S. (2005). Patterns of red muscle strain/activation and body kinematics during steady swimming in a lamnid shark, the shortfin mako (*Isurus oxyrinchus*). *Journal of Experimental Biology* **208**, 2377–2387.

Donley, J. M., Shadwick, R. E., Sepulveda, C. A. & Syme, D. A. (2007). Thermal dependence of contractile properties of the aerobic locomotor muscle in the leopard shark and shortfin mako shark. *Journal of Experimental Biology* **210**, 1194–1203.

Eaton, R. C. & Emberley, D. S. (1991). How stimulus direction determines the trajectory of the Mauthner-initiated escape response in a teleost fish. *Journal of Experimental Biology* **161**, 469–487.

Eaton, R. C., Bombardieri, R. A. & Meyer, D. L. (1977). The Mauthner-initiated startle response in teleost fish. *Journal of Experimental Biology* **66**, 65–81.

Eaton, R. C., Lavender, W. A. & Wieland, C. M. (1981). Identification of Mauthner-initiated response patterns in goldfish: evidence from simultaneous cinematography and electrophysiology. *Journal of Comparative Physiology* **144**, 521–531.

Eaton, R. C., Canfield, J. G. & Guzik, A. L. (1995). Left-right discrimination of sound onset by the Mauthner system. *Brain Behavior and Evolution* **46**, 165–179.

Ellerby, D. J. & Altringham, J. D. (2001). Spatial variation in fast muscle function of the rainbow trout *Oncorhynchus mykiss* during fast-starts and sprinting. *Journal of Experimental Biology* **204**, 2239–2250.

Ferry, L. A. & Lauder, G. V. (1996). Heterocercal tail function in leopard sharks: a three-dimensional kinematic analysis of two models. *Journal of Experimental Biology* **199**, 2253–2268.

Fetcho, J. R. (1991). Spinal network of the Mauthner cell. *Brain Behavior and Evolution* **37**, 298–316.

Fetcho, J. R. & Faber, D. S. (1988). Identification of motoneurons and interneurons in the spinal network for escapes initiated by the Mauthner cell in goldfish. *Journal of Neuroscience* **8**, 4192–4213.

Fierstine, H. L. & Walters, V. (1968). Studies in locomotion and anatomy of scombroid fishes. *Memoirs of the Southern California Academy of Sciences* **6**, 1–31.

Fish, F. E. & Shannahan, L. D. (2000). The role of the pectoral fins in body trim of sharks. *Journal of Fish Biology* **56**, 1062–1073.

Flammang, B. (2010). Functional morphology of the radialis muscle in shark tails. *Journal of Morphology* **271**, 340–352.

Foreman, M. B. & Eaton, R. C. (1993). The direction change concept for reticulospinal control of goldfish escape. *Journal of Neuroscience* **13**, 4101–4113.

Gemballa, S., Ebmeyer, L., Hagen, K., Hannich, T., Hoja, K., Rolf, M., Treiber, K., Vogel, F. & Weitbrecht, G. (2003). Evolutionary transformations of myoseptal tendons in gnathostomes. *Proceedings of the Royal Society B* **270**, 1229–1235.

Gemballa, S., Konstantinidis, P., Donley, J. M., Sepulveda, C. & Shadwick, R. E. (2006). Evolution of high-performance swimming in sharks: transformations of the musculotendinous system from subcarangiform to thunniform swimmers. *Journal of Morphology* **267**, 477–493.

Gillis, G. B. (1998). Neuromuscular control of anguilliform locomotion: patterns of red and white muscle activity during swimming in the American eel *Anguilla rostrata*. *Journal of Experimental Biology* **201**, 3245–3256.

Gleiss, A. C., Gruber, S. H. & Wilson, R. P. (2009). Multi-channel data-logging: towards determination of behaviour and metabolic rate in free-swimming sharks. In *Tagging and Tracking of Marine Animals with Electronic Devices* (Nielsen, J. L. A. H., Fragoso, N., Hobday, A., Lutcavage, M. & Sibert, J., eds), pp. 211–228. Berlin: Springer.

Gleiss, A. C., Dale, J. J., Holland, K. N. & Wilson, R. P. (2010). Accelerating estimates of activity-specific metabolic rate in fishes: testing the applicability of acceleration data-loggers. *Journal of Experimental Marine Biology and Ecology* **385**, 85–91.

Gleiss, A. C., Norman, B. & Wilson, R. P. (2011*a*). Moved by that sinking feeling: variable diving geometry underlies movement strategies in whale sharks. *Functional Ecology* **25**, 595–607.

Gleiss, A. C., Jorgensen, S. J., Liebsch, N., Sala, J. E., Norman, B., Hays, G. C., Quintana, F., Grundy, E., Campagna, C., Trites, A. W., Block, B. A. & Wilson, R. P. (2011*b*). Convergent evolution in locomotory patterns of flying and swimming animals. *Nature Communications* **2**, 352. doi: 10.1038/ncomms1351

Gleiss, A. C., Wilson, R. P. & Shepard, E. L. C. (2011*c*). Making overall dynamic body acceleration work: on the theory of acceleration as a proxy for energy expenditure. *Methods in Ecology and Evolution* **2**, 23–33.

Gore, M. A., Rowat, D., Hall, J., Gell, F. R. & Ormond, R. F. (2008). Transatlantic migration and deep mid-ocean diving by basking shark. *Biology Letters* **4**, 395–398.

Graham, J. B. & Dickson, K. A. (2000). The evolution of thunniform locomotion and heat conservation in scombroid fishes: new insights based on the morphology of *Allothunnus fallai*. *Zoological Journal of the Linnean Society* **129**, 419–466.

Graham, J. B., Dewar, H., Lai, N. C., Lowell, W. R. & Arce, S. M. (1990). Aspects of shark swimming performance determined using a large water tunnel. *Journal of Experimental Biology* **151**, 175–192.

Gray, J. (1933). Studies in animal locomotion I. The movement of fish with special reference to the eel. *Journal of Experimental Biology* **10**, 88–U88.

Greene, C. W. (1913). An undescribed longitudinal differentiation of the great lateral muscle of the king salmon. *Anatomical Record* **7**, 99–101.

Grove, A. J. & Newell, G. E. (1936). A mechanical investigation into the effectual action of the caudal fin in some aquatic chordates. *Annals & Magazine of Natural History Series* **10**, 280–290.

Hale, M. E., Long, J. H., McHenry, M. J. & Westneat, M. W. (2002). Evolution of behavior and neural control of the fast-start escape response. *Evolution* **56**, 993–1007.

Hammerschlag, N., Gallagher, A. J. & Lazarre, D. M. (2011). A review of shark satellite tagging studies. *Journal of Experimental Marine Biology and Ecology* **398**, 1–8.

Harden Jones, F. R. (1973). Tail beat frequency, amplitude, and swimming speed of a shark tracked by sector scanning sonar. *Journal du Conseil international pour l'exploration de la Mer* **35**, 95–97.

Harris, J. E. (1936). The role of the fins in the equilibrium of the swimming fish I. Wind-tunnel tests on a model of *Mustelus canis* (Mitchill). *Journal of Experimental Biology* **13**, 476–493.

Hill, A. V. (1950). The dimensions of animals and their muscular dynamics. *Science Progress* **39**, 209–230.

Hunter, J. R. & Zweifel, J. R. (1971). Swimming speed, tail beat frequency, tail beat amplitude, and size in jack mackerel, *Trachurus symmetricus*, and other fishes. *Fishery Bulletin* **69**, 253–266.

Jayne, B. C. & Lauder, G. V. (1993). Red and white muscle activity and kinematics of the escape response of the bluegill sunfish during swimming. *Journal of Comparative Physiology A* **173**, 495–508.

Jayne, B. C. & Lauder, G. V. (1995). Speed effects on midline kinematics during steady undulatory swimming of largemouth bass, *Micropterus salmoides*. *Journal of Experimental Biology* **198**, 585–602.

Johnson, M. P. & Tyack, P. L. (2003). A digital acoustic recording tag for measuring the response of wild marine mammals to sound. *IEEE Journal of Oceanic Engineering* **28**, 3–12.

Jorgensen, S. J., Reeb, C. A., Chapple, T. K., Anderson, S., Perle, C., Van Sommeran, S. R., Fritz-Cope, C., Brown, A. C., Klimley, A. P. & Block, B. A. (2010). Philopatry and migration of Pacific white sharks. *Proceedings of the Royal Society B* **277**, 679–688.

Kasapi, M. A., Domenici, P., Blake, R. W. & Harper, D. (1993). The kinematics and performance of escape responses of the knifefish. *Canadian Journal of Zoology* **71**, 189–195.

Katz, S. L. (2002). Design of heterothermic muscle in fish. *Journal of Experimental Biology* **205**, 2251–2266.

Katz, S. L. & Shadwick, R. E. (1998). Curvature of swimming fish midlines as an index of muscle strain suggests swimming muscle produces net positive work. *Journal of Theoretical Biology* **193**, 243–256.

Klimley, A. P., Beavers, S. C., Curtis, T. H. & Jorgensen, S. J. (2002). Movements and swimming behavior of three species of sharks in La Jolla Canyon, California. *Environmental Biology of Fishes* **63**, 117–135.

Kohashi, T. & Oda, Y. (2008). Initiation of mauthner- or non-mauthner-mediated fast escape evoked by different modes of sensory input. *Journal of Neuroscience* **28**, 10641–10653.

Korn, H. & Faber, D. S. (2005). The Mauthner cell half a century later: a neurobiological model for decision-making? *Neuron* **47**, 13–28.

Kryvi, H. & Eide, A. (1977). Morphometric and autoradiographic studies on growth of red and white axial muscle fibers in the shark *Etmopterus spinax*. *Anatomy and Embryology* **151**, 17–28.

Kryvi, H. & Totland, G. K. (1977). Histochemical studies with microphotometric determinations of the lateral muscles in the sharks *Etmopterus spinax* and *Galeus melastomus*. *Journal of the Marine Biological Association of the United Kingdom* **57**, 261–271.

Kryvi, H., Flatmark, T. & Totland, G. K. (1981). The myoglobin content in red, intermediate and white fibers of the swimming muscles in 3 species of shark: a comparative study using high performance liquid chromatography. *Journal of Fish Biology* **18**, 331–338.

Lacey, C., Leaper, R., Moscrop, A., Gillespie, D., McLanaghan, R. & Brown, S. (2010). Photo-grammetric measurements of swimming speed and body length of basking sharks observed around the Hebrides, Scotland. *Journal of the Marine Biological Association of the United Kingdom* **90**, 361–366.

Lighthill, M. J. (1970). Aquatic animal propulsion of high hydromechanical efficiency. *Journal of Fluid Mechanics* **44**, 265–301.

Lingham-Soliar, T. (2005). Caudal fin in the white shark, *Carcharodon carcharias* (Lamnidae): a dynamic propeller for fast, efficient swimming. *Journal of Morphology* **264**, 233–252.

Lou, F., Curtin, N. A. & Woledge, R. (2002). Isometric and isovelocity contractile performance of red muscle fibres from the dogfish *Scyliorhinus canicula*. *Journal of Experimental Biology* **205**, 1585–1595.

Lowe, C. G. (1996). Kinematics and critical swimming speed of juvenile scalloped hammerhead sharks. *Journal of Experimental Biology* **199**, 2605–2610.

Lowe, C. G. (2002). Bioenergetics of free-ranging juvenile scalloped hammerhead sharks (*Sphyrna lewini*) in Kane'ohe Bay, O'ahu, HI. *Journal of Experimental Marine Biology and Ecology* **278**, 141–156.

Lowe, C. G. & Goldman, K. J. (2001). Thermal and bioenergetics of elasmobranchs: bridging the gap. *Environmental Biology of Fishes* **60**, 251–266.

Martin, A. P. (1996). Systematics of the Lamnidae and the origination time of *Carcharodon carcharias* inferred from the comparative analysis of mitochondrial DNA sequences. In *Great White Shark. The Biology of Carcharodon carcharias*. (Klimley, A. P. & Ainley, D. G., eds.), pp. 49–59. San Diego, CA: Academic Press.

McClellan, A. D. & Grillner, S. (1983). Initiation and sensory gating of 'fictive' swimming and withdrawal responses in an in vitro preparation of the lamprey spinal cord. *Brain Research* **269**, 237–250.

Meyer, C. G., Clark, T. B., Papastamatiou, Y. P., Whitney, N. M. & Holland, K. N. (2009). Long-term movement patterns of tiger sharks *Galeocerdo cuvier* in Hawaii. *Marine Ecology Progress Series* **381**, 223–235.

Muramoto, H., Ogawa, M., Suzuki, M. & Naito, Y. (2004). Little Leonardo digital data logger: its past, present and future role in bio-logging science. *Memoirs of National Institute of Polar Research Special Issue* **58**, 196–202.

Nakamura, I., Watanabe, Y. Y., Papastamatiou, Y. P., Sato, K. & Meyer, C. G. (2011). Yo-yo vertical movements suggest a foraging strategy for tiger sharks *Galeocerdo cuvier*. *Marine Ecology Progress Series* **424**, 237–246.

Nissanov, J. & Eaton, R. C. (1989). Reticulospinal control of rapid escape turning maneuvers in fishes. *American Zoologist* **29**, 103–121.

Nursall, J. R. (1956). The lateral musculature and the swimming of fish. *Proceedings of the Zoological Society of London* **126**, 127–143.

Papastamatiou, Y. P., Cartamil, D. P., Lowe, C. G., Meyer, C. G., Wetherbee, B. M. & Holland, K. N. (2011). Scales of orientation, directed walks and movement path structure in sharks. *Journal of Animal Ecology* **80**, 864–874.

Perry, C. N., Cartamil, D. P., Bernal, D., Sepulveda, C. A., Theilmann, R. J., Graham, J. B. & Frank, L. R. (2007). Quantification of red myotomal muscle volume and geometry in the shortfin mako shark (*Isurus oxyrinchus*) and the salmon shark (*Lamna ditropis*) using T-1-weighted magnetic resonance imaging. *Journal of Morphology* **268**, 284–292.

Reif, W.-E., Weishampel, D. B. (1986). Anatomy and mechanics of the lunate tail in lamnid sharks. *Zoologische Jahrbücher. Abtheilung für Anatomie und Ontogenie der Thiere* **114**, 221–234.

Ropert-Coudert, Y., Beaulieu, M., Hanuise, N. & Kato, A. (2010). Diving into the world of biologging. *Endangered Species Research* **10**, 21–27.

Rovainen, C. M. (1978). Müller cells, "Mauthner" cells and other identified reticulospinal neurons in the lamprey. In *Neurobiology of the Mauthner Cell* (Faber, D. S. & Korn, H., eds), pp. 245–269. New York, NY: Raven Press.

Rovainen, C. M. (1983). Identified neurons in the lamprey spinal cord and their roles in fictive swimming. *Symposia of the Society for Experimental Biology* **37**, 305–330.

Rutz, C. & Hays, G. C. (2009). New frontiers in biologging science. *Biology Letters* **5**, 289–292.

Sato, K., Watanuki, Y., Takahashi, A., Miller, P. J. O., Tanaka, H., Kawabe, R., Ponganis, P. J., Handrich, Y., Akamatsu, T., Watanabe, Y., Mitani, Y., Costa, D. P., Bost, C. A., Aoki, K., Amano, M., Trathan, P., Shapiro, A. & Naito, Y. (2007). Stroke frequency, but not swimming speed, is related to body size in free-ranging seabirds, pinnipeds and cetaceans. *Proceedings of the Royal Society B* **274**, 471–477.

Sato, K., Shiomi, K., Watanabe, Y., Watanuki, Y., Takahashi, A. & Ponganis, P. J. (2010). Scaling of swim speed and stroke frequency in geometrically similar penguins: they swim optimally to minimize cost of transport. *Proceedings of the Royal Society B* **277**, 707–714.

Saunders, R. A., Royer, F. & Clarke, M. W. (2011). Winter migration and diving behaviour of porbeagle shark, *Lamna nasus*, in the Northeast Atlantic. *ICES Journal of Marine Science* **68**, 166–174.

Schmidt-Nielsen, K. (1984). *Scaling: Why is Animal Size so Important?* Cambridge: Cambridge University Press.

Sepulveda, C. A., Kohin, S., Chan, C., Vetter, R. & Graham, J. B. (2004). Movement patterns, depth preferences, and stomach temperatures of free-swimming juvenile mako sharks, *Isurus oxyrinchus*, in the Southern California Bight. *Marine Biology* **145,** 191–199.

Sepulveda, C. A., Wegner, N. C., Bernal, D. & Graham, J. B. (2005). The red muscle morphology of the thresher sharks (family Alopiidae). *Journal of Experimental Biology* **208**, 4255–4261.

Sepulveda, C. A., Graham, J. B. & Bernal, D. (2007). Aerobic metabolic rates of swimming mako sharks, *Isurus oxyrinchus*. *Marine Biology* **152**, 1087–1094.

Shadwick, R. E. (2005). How tunas and lamnid sharks swim: an evolutionary convergence. *American Scientist* **93**, 524–531.

Shadwick, R. E. & Gemballa, S. (2006). Structure, kinematics, and muscle dynamics in undulatory swimming. In *Fish Biomechanics* (Shadwick, R. E. & Lauder, G. V., eds), pp. 241–280. San Diego, CA: Elsevier Academic Press.

Shadwick, R. E., Steffensen, J. F., Katz, S. L. & Knower, T. (1998). Muscle dynamics in fish during steady swimming. *American Zoologist* **38**, 755–770.

Shiomi, K., Sato, K., Mitamura, H., Arai, N., Naito, Y. & Ponganis, P. J. (2008). Effect of ocean current on the dead-reckoning estimation of 3-D dive paths of emperor penguins. *Aquatic Biology* **3**, 265–270.

da Silva, C., Kerwath, S. E., Wilke, C. G., Meyer, M. & Lamberth, S. J. (2010). First documented southern transatlantic migration of a blue shark *Prionace glauca* tagged off South Africa. *African Journal of Marine Science* **32**, 639–642.

Sims, D. W. (1999). Threshold foraging behaviour of basking sharks on zooplankton: life on an energetic knife-edge? *Proceedings of the Royal Society B* **266**, 1437–1443.

Sims, D. W. (2000). Filter-feeding and cruising swimming speeds of basking sharks compared with optimal models: they filter-feed slower than predicted for their size. *Journal of Experimental Marine Biology and Ecology* **249**, 65–76.
Sims, D. W. & Quayle, V. A. (1998). Selective foraging behaviour of basking sharks on zooplankton in a small-scale front. *Nature* **393**, 460–464.
Skomal, G. B., Zeeman, S. I., Chisholm, J. H., Summers, E. L., Walsh, H. J., McMahon, K. W. & Thorrold, S. R. (2009). Transequatorial migrations by basking sharks in the western Atlantic ocean. *Current Biology* **19**, 1019–1022.
Sundström, L. F. & Gruber, S. H. (1998). Using speed-sensing transmitters to construct a bioenergetics model for subadult lemon sharks, *Negaprion brevirostris* (Poey), in the field. *Hydrobiologia* **371–372**, 241–247.
Sundström, L. F. & Gruber, S. H. (2002). Effects of capture and transmitter attachments on the swimming speed of large juvenile lemon sharks in the wild. *Journal of Fish Biology* **61**, 834–838.
Sundström, L. F., Gruber, S. H., Clermont, S. M., Correia, J. P. S., de Marignac, J. R. C., Morrissey, J. F., Lowrance, C. R., Thomassen, L. & Oliveira, M. T. (2001). Review of elasmobranch behavioral studies using ultrasonic telemetry with special reference to the lemon shark, *Negaprion brevirostris*, around Bimini Islands, Bahamas. *Environmental Biology of Fishes* **60**, 225–250.
Syme, D. A. (2006). Functional properties of skeletal muscle. In *Fish Biomechanics* (Shadwick, R. E. & Lauder, G. V., eds.), pp. 179–240. San Diego, CA: Elsevier Academic Press.
Syme, D. A. & Shadwick, R. E. (2011). Red muscle function in stiff-bodied swimmers: there and almost back again. *Philosophical Transactions of the Royal Society B* **366**, 1507–1515.
Thomson, K. S. (1976). On the heterocercal tail in sharks. *Paleobiology* **2**, 19–38.
Thomson, K. S. & Simanek, D. E. (1977). Body form and locomotion in sharks. *American Zoologist* **17**, 343–354.
Totland, G. K., Kryvi, H., Bone, Q. & Flood, P. R. (1981). Vascularisation of the lateral muscle of some elasmobranchiomorph fishes. *Journal of Fish Biology* **18**, 223–234.
Triantafyllou, G. S., Triantafyllou, M. S. & Grosenbaugh, M. A. (1993). Optimal thrust development in oscillating foils with an application to fish propulsion. *Journal of Fluids and Structures* **7**, 205–224.
Tytell, E. D. & Lauder, G. V. (2002). The C-start escape response of *Polypterus senegalus*: bilateral muscle activity and variation during stage 1 and 2. *Journal of Experimental Biology* **205**, 2591–2603.
Videler, J. J. (1993). *Fish Swimming*. London: Chapman & Hall.
Wainwright, S. A. (1983). To bend a fish. In *Fish Biomechanics* (Webb. P. & Weihs, D., eds), pp. 68–91. New York, NY: Praeger.
Wakeling, J. M. (2001). Biomechanics of fast-start swimming in fish. *Comparative Biochemistry and Physiology A* **131**, 31–40.
Wakeling, J. M. & Johnston, I. A. (1998). Muscle power output limits fast-start performance in fish. *Journal of Experimental Biology* **201**, 1505–1526.
Wakeling, J. M. & Johnston, I. A. (1999). Body bending during fast-starts in fish can be explained in terms of muscle torque and hydrodynamic resistance. *Journal of Experimental Biology* **202**, 675–682.
Wakeling, J. M., Kemp, K. M. & Johnston, I. A. (1999). The biomechanics of fast-starts during ontogeny in the common carp *Cyprinus carpio*. *Journal of Experimental Biology* **202**, 3057–3067.
Wardle, C. S., Videler, J. J. & Altringham, J. D. (1995). Tuning in to fish swimming waves: body form, swimming mode and muscle function. *Journal of Experimental Biology* **198**, 1629–1636.
Ware, C., Arsenault, R. & Plumlee, M. (2006). Visualizing the underwater behavior of humpback whales. *IEEE Computer Graphics and Applications* **26**, 14–18.
Ware, C., Friedlaender, A. S. & Nowacek, D. P. (2010). Shallow and deep lunge feeding of humpback whales in fjords of the West Antarctic Peninsula. *Marine Mammal Science* **27**, 587–605.

Watanabe, Y. Y., Sato, K., Watanuki, Y., Takahashi, A., Mitani, Y., Amano, M., Aoki, K., Narazaki, T., Takashi, I., Minamikawa, S. & Miyazaki, N. (2010). Scaling of swim speed in breath-hold divers. *Journal of Animal Ecology* **80**, 57–68.
Webb, P. W. (1975). Acceleration performance of rainbow trout *Salmo gairdneri* and green sunfish *Lepomis cyanellus*. *Journal of Experimental Biology* **63**, 451–465.
Webb, P. W. (1978). Fast-start performance and body form in seven species of teleost fish. *Journal of Experimental Biology* **74**, 211–226.
Webb, P. W. & Keyes, R. S. (1982). Swimming kinematics of sharks. *Fishery Bulletin* **80**, 803–812.
Webb, P. W., Kostecki, P. T. & Stevens, E. D. (1984). The effect of size and swimming speed on locomotor kinematics of rainbow trout. *Journal of Experimental Biology* **109**, 77–95.
Wegner, N. C., Sepulveda, C. A., Olson, K. R., Hyndman, K. A. & Graham, J. B. (2010). Functional morphology of the gills of the shortfin mako, *Isurus oxyrinchus*, a lamnid shark. *Journal of Morphology* **271**, 937–948.
Weihs, D. (1973). The mechanism of rapid starting of slender fish. *Biorheology* **10**, 343–350.
Weihs, D., Keyes, R. S. & Stalls, D. M. (1981). Voluntary swimming speeds of two species of large carcharhinid sharks. *Copeia* **1981**, 219–222.
Weng, K. C., Castilho, P. C., Morrissette, J. M., Landeira-Fernandez, A. M., Holts, D. B., Schallert, R. J., Goldman, K. J. & Block, B. A. (2005). Satellite tagging and cardiac physiology reveal niche expansion in salmon sharks. *Science* **310**, 104–106.
Weng, K. C., Boustany, A. M., Pyle, P., Anderson, S. D., Brown, A. & Block, B. A. (2007). Migration and habitat of white sharks (*Carcharodon carcharias*) in the eastern Pacific Ocean. *Marine Biology* **152**, 877–894.
Westneat, M. W. & Wainwright, S. A. (2001). Mechanical design for swimming; muscle, tendon and bone. In *Tuna: Physiology, Ecology and Evolution* (Block, B. A. & Stevend, E. D., eds), pp. 271–311. San Diego, CA: Academic Press.
Westneat, M. W., Hoese, W., Pell, C. A. & Wainwright, S. A. (1993). The horizontal septum: mechanisms of force transfer in locomotion of scombrid fishes (Scombridae: Perciformes). *Journal of Morphology* **217**, 183–204.
Westneat, M. W., Hale, M. E., McHenry, M. J. & Long, J. H. (1998). Mechanics of the fast-start: muscle function and the role of intramuscular pressure in the escape behavior of *Amia calva* and *Polypterus palmas*. *Journal of Experimental Biology* **201**, 3041–3055.
Whitney, N. M., Pratt, H. L. Jr., Pratt, T. C. & Carrier, J. C. (2010). Identifying shark mating behaviour using three-dimensional acceleration loggers. *Endangered Species Research* **10**, 71–82.
Wilga, C. D. & Lauder, G. V. (2000). Three-dimensional kinematics and wake structure of the pectoral fins during locomotion in leopard sharks *Triakis semifasciata*. *Journal of Experimental Biology* **203**, 2261–2278.
Wilga, C. D. & Lauder, G. V. (2002). Function of the heterocercal tail in sharks: quantitative wake dynamics during steady horizontal swimming and vertical maneuvering. *Journal of Experimental Biology* **205**, 2365–2374.
Wilga, C. D. & Lauder, G. V. (2004). Biomechanics - hydrodynamic function of the shark's tail. *Nature* **430**, 850.
Wilson, D. M. (1959). Function of giant mauthner's neurons in the lungfish. *Science* **129**, 841–842.